Helsinki University of Technology
Department of Biomedical Engineering and Computational Science Publications
Teknillisen korkeakoulun Lääketieteellisen tekniikan ja laskennallisen tieteen laitoksen julkaisuja
September 2009 REPORT A12

ACCURATE MODELLING OF TISSUE PROPERTIES IN DIFFUSE OPTICAL IMAGING OF THE HUMAN BRAIN

Juha Heiskala

Dissertation for the degree of Doctor of Science in Technology to be presented with due permission of the Faculty of Information and Natural Sciences for public examination and debate in Auditorium TU2 at Helsinki University of Technology (Espoo, Finland) on the 19th of September, 2009, at 12 o'clock noon.

Helsinki University of Technology
Faculty of Information and Natural Sciences
Department of Biomedical Engineering and Computational Science

Teknillinen korkeakoulu
Informaatio- ja luonnontieteiden tiedekunta
Lääketieteellisen tekniikan ja laskennallisen tieteen laitos

BioMag Laboratory
HUSLAB, Helsinki University Central Hospital

BioMag-laboratorio
HUSLAB, Helsingin yliopistollinen keskussairaala

Distribution:
Helsinki University of Technology
Department of Biomedical Engineering and Computational Science
http://www.becs.tkk.fi
P.O. Box 3310
FI-02015 TKK
FINLAND

Tel. +358 9 451 3172
Fax +358 9 451 3182
http://www.becs.tkk.fi

Online in PDF format: http://lib.tkk.fi/Diss/2009/isbn9789522480590

E-mail: juha.heiskala@iki.fi

ISBN 978-952-248-058-3 (print)
ISBN 978-952-248-059-0 (PDF)
ISSN 1797-3996 (paper)

Picaset Oy
Helsinki 2009

ABSTRACT OF DOCTORAL DISSERTATION	HELSINKI UNIVERSITY OF TECHNOLOGY P. O. BOX 1000, FI-02015 TKK http://www.tkk.fi

Author Juha Heiskala

Name of the dissertation

Accurate modelling of tissue properties in diffuse optical imaging of the human brain

Manuscript submitted 20.4.2009	Manuscript revised 30.8.2009
Date of the defence 19.9.2009	
☐ Monograph	☒ Article dissertation (summary + original articles)

Faculty	Faculty of Information and Natural Sciences
Department	Department of Biomedical Engineering and Computational Science
Field of research	Medical imaging, biomedical optics
Opponent(s)	Rainer Macdonald, Professor, PhD, PTB Berlin
Supervisor	Risto Ilmoniemi, Professor, D.Sc
Instructor	Ilkka Nissilä, D.Sc

Abstract

Diffuse optical imaging (DOI) is an emerging imaging modality for non-invasive functional medical imaging, using near infrared (NIR) or visible red light. The innovation is to derive functional information about living tissue from measurements of light that has passed through it. Optical imaging can be applied to imaging of tissues as diverse as the central nervous system, female breast, muscle, and joints of fingers. This thesis addresses the application of DOI to studying the human brain.

In this thesis, the problems of modelling light propagation in the adult and infant human head, and reconstructing three-dimensional images of functional changes in the brain using optical measurements, are addressed. *Difference imaging*, where changes from baseline optical parameters rather than absolute parameter values are reconstructed, is considered. The goal was to develop methods for accurate modelling of light propagation and to clarify how specific aspects of the computational modelling affect the reconstruction of functional images from optical measurements of the human brain. Specifically, the significance of anisotropic light propagation in the white matter, and *a priori* knowledge of the anatomy and the optical properties of the head and brain are studied. Moreover, a generic probabilistic *atlas* model of the infant head to enhance image reconstruction is developed.

Significance of anisotropic light propagation was found to be small in optical imaging of the adult brain. Although anisotropic light propagation may have a larger impact on the measured signal when infants are imaged, results suggest that image reconstruction can be performed without taking anisotropy into consideration.

The use of *a priori* anatomical knowledge was found to significantly improve the accuracy and robustness of image reconstruction in difference imaging. The results suggest that for optimal reconstructions, individual MR imaging based anatomical data should be used when possible. For cases where individual anatomical data is not available, atlas models should be developed. An important consideration is how to obtain the baseline optical parameters of tissue classes in the anatomical model. Literature-derived parameters can be used as a starting point. For optimal results however, methods should be developed for estimating the baseline parameters from measured data.

Keywords diffuse optical imaging, monte carlo, biomedical optics

ISBN (printed) 978-952-248-058-3	ISSN (printed) 1797-3996
ISBN (pdf) 978-952-248-059-0	ISSN (pdf)
Language English	Number of pages 158

Publisher Department of Biomedical Engineering and Computational Science, Helsinki University of Technology

Print distribution Helsinki University of Technology, Dept. of Biomedical Engineering and Computational Science

☒ The dissertation can be read at http://lib.tkk.fi/Diss/2009/isbn9789522480590

VÄITÖSKIRJAN TIIVISTELMÄ	TEKNILLINEN KORKEAKOULU PL 1000, 02015 TKK http://www.tkk.fi

Tekijä Juha Heiskala

Väitöskirjan nimi

Tarkka mallintaminen ihmisaivojen diffuusissa optisessa kuvantamisessa

Käsikirjoituksen päivämäärä 20.4.2009	Korjatun käsikirjoituksen päivämäärä 30.8.2009
Väitöstilaisuuden ajankohta 19.9.2009	
☐ Monografia	☒ Yhdistelmäväitöskirja (yhteenveto + erillisartikkelit)

Tiedekunta	Informaatio- ja luonnontieteiden tiedekunta
Laitos	Lääketieteellisen tekniikan ja laskennallisen tieteen laitos
Tutkimusala	Lääketieteellinen tekniikka, optinen kuvantaminen
Vastaväittäjä(t)	Prof. Rainer Macdonald, PTB Berlin
Työn valvoja	Prof. Risto Ilmoniemi
Työn ohjaaja	TkT Ilkka Nissilä

Tiivistelmä

Diffuusi optinen kuvantaminen on verrattain uusi funktionaalinen lääketieteellinen kuvantamismenetelmä, joka hyödyntää infrapuna- ja näkyvää punaista valoa. Mittaamalla kudoksen läpi kulkenutta valoa saadaan tietoa fysiologisista parametreista, kuten hemoglobiinin konsentraatiosta. Optista kuvantamista voidaan käyttää muunmuassa keskushermoston, lihaksiston, naisen rintakudoksen ja nivelten tutkimiseen. Tämän väitöstyön aiheena on diffuusin optisen kuvantamisen soveltaminen ihmisaivojen toiminnan tutkimiseen.

Työssä tutkittiin aikuisen ja lapsen aivojen optisessa kuvantamisessa tarvittavaa mallintamista ja aivotoiminnan aiheuttamien verenkierron muutosten paikantamisessa ja kvantifioinnissa (rekonstruktiossa) tarvittavia menetelmiä. Muutosten rekonstruointi on *differenssikuvantamista*, jossa pyritään määrittämään optisissa parametreissa tapahtuvia muutoksia parametrien absoluuttisten arvojen sijaan. Työn tavoitteena oli kehittää menetelmiä infrapunavalon etenemisen tarkaksi mallintamiseksi sekä selvittää, miten mallin yksityiskohdat vaikuttavat rekonstruktion onnistumiseen. Erityisenä huomion kohteena olivat aivojen valkean aineen epäisotrooppisen sironnan mallintaminen sekä anatomisen *a priori*-tiedon käyttäminen mallintamisessa ja rekonstruktiossa. Työssä kehitettiin yleistä anatomista *a priori*-tietoa sisältävä *atlas*-malli vastasyntyneen lapsen päästä.

Epäisotrooppisen sironnan vaikutus aikuisen aivojen funktionaaliseen kuvantamiseen optisin menetelmin havaittiin tutkimuksessa pieneksi. Pienten lasten kuvantamisessa epäisotropia voi havaittavasti vaikuttaa mitattavaan optisen signaaliin, mutta funktionaalisten muutosten rekonstruktiossa sen merkitys on pieni.

Anatomisen *a priori*-tiedon käyttö rekonstruktion apuna differenssikuvantamisessa havaittiin hyödylliseksi. Tulosten perusteella rekonstruktion tukena olisi pyrittävä käyttämään mahdollisuuksien mukaan potilaan tai koehenkilön omasta MR-kuvasta saatavaa anatomista tietoa, tai jos tämä ei ole mahdollista, atlas-mallista saatavaa yleistä anatomista tietoa. Anatomisen tiedon lisäksi laskentaan tarvitaan kudostyyppien optisten taustaparametrien arvot. Kirjallisuusarvojen käyttäminen on mahdollista, mutta rekonstruktiotulosten luotettavuuden ja tarkkuuden parantamiseksi olisi kehitettävä menetelmiä, joiden avulla taustaparametrien arvot voidaan määrittää mittausdatan perusteella

Asiasanat diffuusi optinen kuvantaminen, monte carlo

ISBN (painettu) 978-952-248-058-3	ISSN (painettu) 1797-3996
ISBN (pdf) 978-952-248-059-0	ISSN (pdf)
Kieli englanti	Sivumäärä 158

Julkaisija Lääketieteellisen tekniikan ja laskennallisen tieteen laitos, Teknillinen korkeakoulu

Painetun väitöskirjan jakelu Teknillinen korkeakoulu, Lääketieteellisen tekniikan ja laskennallisen tieteen laitos

☒ Luettavissa verkossa osoitteessa http://lib.tkk.fi/Diss/2009/isbn9789522480590

Preface

This work was carried out in the BioMag laboratory at the Helsinki University Central Hospital, in close collaboration with the research group of biomedical optics of the Department of Biomedical Engineering and Computational Science of the Helsinki University of Technology. The financial support of the Finnish Foundation for Technology Promotion, the Finnish Cultural Foundation, the Instrumentarium Science Foundation, the Vilho, Yrjö and Kalle Väisälä Foundation of the Finnish Academy of Science and Letters, the KAUTE Foundation, the Biomedicum Helsinki Foundation, the Alfred Kordelin Foundation, and the graduate school Functional Research in Medicine are acknowledged.

I am much indebted to my thesis instructor Dr. Ilkka Nissilä, with whom I have spent numerous late nights in the laboratory trying to get some manuscript finished before the dead line. I am also grateful to the former head of the BioMag laboratory and current head of the Department of Biomedical Engineering and Computational Science of the Helsinki University of Technology Prof. Risto Ilmoniemi for employing me in the BioMag laboratory and teaching me about academic freedom and the responsibility that comes with it. I thank the current head of the BioMag laboratory Jyrki Mäkelä for providing a relaxed and productive atmosphere, and practical help on occasions that it was needed. I greatly appreciated the collaboration of Prof. Erkki Somersalo in the early stages of my thesis work. I would also like to express gratitude for the support over the years of Professors Risto Ilmoniemi and Pekka Meriläinen and Prof. emeritus Toivo Katila for the group of biomedical optics.

I would like to thank Prof. Simon Arridge of the University College London for taking me in his laboratory for a period of three months during my thesis work, and for the many helpful discussions about optical tomography during and after that time.

I am grateful to Prof. Jari Kaipio and Prof. Alwin Kienle for their careful review of my thesis and their constructive criticism and suggestions for improvements.

Scientific work cannot be carried out alone, and I would like to thank all my co-authors and collaborators. I would especially like to mention Tuomas Neuvonen, with whom I have discussed scientific matters on numerous occasions, and matters completely unrelated to science even more often. At the Helsinki University of Technology, the current and former members of the group of biomedical optics, Kalle Kotilahti, Jenni Heino, Tommi Noponen, Lauri Lipiäinen, Petri Hiltunen, Tiina Näsi, Jaakko Virtanen, Atte Lajunen and Hanna Mustaniemi have always welcomed me for a discussion, scientific or otherwise. Outside the medical optics group, the collaboration with Mika Pollari has been very pleasurable and also productive.

The people of the BioMag laboratory have made working there pleasurable. I have very fond memories of the times with my former office mates Jussi Nurminen, Ville Mäkinen and Simo Monto. I have also much appreciated the company of Elina Pihko, Päivi Nevalainen, Ville Mäntynen, Pantelis Lioumis, Dubravko Kicic, Leena Lauronen, Satu and Matias Palva, Essi Rossi, Pirjo Kari, Juha Montonen, and the rest of the lovely people who are too numerous to be all mentioned by name. You make BioMag what it is.

Finally, I would like to thank my dear family for all their support, and my friends for helping me on occasion to forget all about science and work, and enjoy the life outside the laboratory.

London, August 30, 2009

Juha Heiskala

Contents

List of Publications

This thesis consists of an overview and of the following publications which are referred to in the text by their Roman numerals.

I J. Heiskala, I. Nissilä, T. Neuvonen, S. Järvenpää, and E. Somersalo, "Modeling anisotropic light propagation in a realistic model of the human head," Applied Optics **44**, 2049-2057 (2005)

II J. Heiskala, T. Neuvonen, P. E. Grant, and I. Nissilä, "Significance of tissue anisotropy in optical tomography of the infant brain," Applied Optics **46**, 1633-1640 (2007)

III J. Heiskala, K. Kotilahti, and I. Nissilä, "An application of perturbation Monte Carlo in optical tomography", Proc. IEEE Eng. in Medicine and Biology, **27**, 274-277 (2005)

IV J. Heiskala, K. Kotilahti, L. Lipiäinen, P. Hiltunen, P. E. Grant, and I. Nissilä, "Optical tomographic imaging of activation of the infant auditory cortex using perturbation Monte Carlo with anatomical a priori information", in *Diffuse Optical Imaging in Tissue*, B. W. Pogue and R. Cubeddu, eds. Proc. SPIE **6629**, paper 66290T (2007) (11 pages)

V J. Heiskala, P. Hiltunen, and I. Nissilä, "Significance of background optical properties, time-resolved information, and optode arrangement in diffuse optical imaging of term neonates", Phys. Med. Biol. **54**, 535-554 (2009)

VI J. Heiskala, M. Pollari, M. Metsäranta, P. E. Grant, and I. Nissilä, "Probabilistic atlas can improve reconstruction from optical imaging of the neonatal brain", Opt. Express **17**, 14977-14992 (2009)

Author's contribution

All publications in this thesis are the result of shared work of all co-authors. In all the publications, I have taken the main responsibility for writing the manuscripts, while taking into account the useful comments and suggestions of my co-authors. I implemented the Monte Carlo (MC) modelling and created the various anatomical models used throughout the publications. In the following, I state my contribution in each publication in more detail.

Publication I: I wrote almost the entirety of the manuscript and created the images for all figures. I designed the new method for handling anisotropy in radiative transfer equation and did the mathematical derivation of the corresponding anisotropic diffusion approximation. I also implemented the MC code with extension to anisotropy. I segmented the anatomical T1-weighted MR image used in the manuscript. I derived the way DT-MRI data could be used for estimating the optical anisotropy, and did the coregistration of the T1 and DT MR images together with the third co-author. I designed the simulated experiments and analyzed the results together with the second co-author.

Publication II: I wrote almost the entirety of the manuscript, and created the images. I segmented the T1-weighted MR images, and performed the coregistration of the T1 and DT-MR images together with the second co-author. I implemented the MC code for calculating the spatial pattern of sensitivity of the optical measurement. I designed the simulated experiments together with the fourth co-author, and analyzed the results.

Publication III: I was mainly responsible for writing the manuscript, and created all the images. I segmented the MR image and created the anatomical model based on the segmentation. I implemented the perturbation Monte Carlo (pMC) code, per-

formed the simulated measurement, and computed the pMC image reconstructions from both simulated and measured data.

Publication IV: I was mainly responsible for writing the manuscript, and created most of the images. I created the anatomical models based on MR images I had previously segmented. I participated in the experiments and implemented the simulated measurements with MC. I implemented the perturbation Monte Carlo (pMC) code, and computed the pMC image reconstructions from both simulated and measured data.

Publication V: I was mainly responsible for writing the manuscript, and created all of the images. I implemented the pMC method used in the manuscript. I designed the simulated experiments together with the third co-author. I implemented the simulated measurements and performed the pMC based image reconstructions. I designed the quantitative measures of image quality with the third co-author, and implemented them.

Publication VI: I was mainly responsible for writing the manuscript, and created all of the images. I designed the probabilistic atlas together with the fifth co-author and segmented the MR images using interactive software written by the fith co-author. I coregistered the MR images together with the second co-author. I designed and implemented the MC methodology which was compatible with the atlas model. I designed the simulated experiments together with the fifth co-author, implemented the simulated measurements, and performed the pMC based image reconstructions. I designed the quantitative measures of image quality with the fifth co-author, and implemented them.

List of Abbreviations

The acronyms and abbreviations used in the overview are listed below.

2D	Two-dimensional
3D	Three-dimensional
BOLD	Blood oxygen level dependent (MRI)
CNR	Contrast-to-noise ratio
CSF	Cerebrospinal fluid
CT	Computed tomography
CW	Continuous wave
DE	Diffusion equation
DOI	Diffuse optical imaging
DPF	Differential pathlength factor
EEG	Electroencephalography
FD	Frequency domain
FE	Finite element
FEM	Finite element method
FISP	Fast imaging with steady-state precession (MRI)
FLASH	Fast low angle shot (MRI)
fMRI	Functional MRI
FVM	Finite volume method
HbO_2	Oxygenated hemoglobin
HbR	Deoxygenated hemoglobin
MC	Monte Carlo
MEG	Magnetoencephalography
MRI	Magnetic resonance imaging
NIRS	Near-infrared spectroscopy
PET	Positron emission tomography
pMC	Perturbation Monte Carlo
RTE	Radiative transport equation
SPECT	Single photon emission computed tomography
TD	Time domain
TPSF	Temporal point spread function

List of Symbols

The most important symbols used in the overview are listed below.

μ_a	Absorption coefficient
μ_s	Scattering coefficient
μ_s'	Reduced scattering coefficient
κ_0	Diffusion coefficient
λ	Wavelength
Θ	Scattering phase function
c	Speed of light
g	Anisotropy factor
n	Refractive index
$\mathbf{J}$	Jacobian matrix

1 Introduction

Diffuse optical imaging (DOI) is an emerging modality for non-invasive functional medical imaging, using near infrared or visible red light. The innovation is to derive information about living tissue from measurements of light that has passed through it. The method can be applied to tissues as diverse as the central nervous system, female breast, muscle, and joints of fingers. This thesis addresses the application of DOI to studying the brain, the most complicated and arguably the most intriguing organ of the human body.

Due to the complex diffusive propagation of near-infrared light in most tissues, recovering the optical parameters, from which functional information can be derived, is a challenging task. Functional optical imaging of the brain can be performed using simple assumptions of the light propagation, but in order to obtain reliable and accurate imaging results, adequate computational models must be used.

In this thesis, the problems of modelling light propagation in the adult and infant human head, and reconstructing three-dimensional images of functional changes in the brain using near infrared optical measurements, are addressed. The goal was to develop methods for accurate modelling of light propagation, and to clarify, how specific aspects of the computational modelling affect the reconstruction of functional images. Specifically, the significance of anisotropic light propagation and *a priori* knowledge of the anatomy and optical properties of the head and brain for obtaining accurate reconstructions were studied. Moreover, a generic probabilistic *atlas* model of the infant head for enhancing image reconstruction was developed. Different aspects of the image reconstruction and modelling are discussed in the six publications included in this thesis.

The thesis is organized as follows. After this introductory section, Section 2 gives

an overview of the field of medical imaging and the place of DOI in this context. Section 3 introduces the physics of diffuse optical imaging, and discusses modelling that is needed to estimate physiological parameters based on optical measurements. Section 4 deals with the development of optical models of the head that can be used for reconstructing images of brain activation. References are made to the results of the publications in this thesis. Finally, Section 5 presents the conclusions made from the research in this thesis are presented. Section 6 summarizes the main results of the publications.

2 Background

2.1 Imaging of human brain function

Medical imaging has gone through rapid development during the last three decades, and numerous methods are available for both anatomical and functional imaging of the human head and brain.

Computed tomography (CT) [1] can provide high resolution anatomical images of the head. With magnetic resonance imaging (MRI) [1], even higher resolution, and better contrast between different types of healthy tissue in the brain, and between healthy and diseased brain tissue, can be obtained. Functional MR imaging (fMRI) [2] can show hemodynamic responses to brain activation via blood oxygen level dependent (BOLD) signal. Nuclear medicine methods, such as positron emission tomography (PET) [1], and single photon emission computed tomography (SPECT) [1], can provide information about brain function by tracing radioactively labeled metabolites. Doppler ultrasound can be used for measuring flow in arteries which provide the brain with its blood supply. Information about the electrical activity of the brain can be obtained using electroencephalography (EEG) and magnetoencephalography (MEG) [3, 4].

Diffuse optical imaging (DOI) and near-infrared spectroscopy (NIRS) can be used to obtain information about the blood volume and oxygenation in the brain. While it is possible to obtain anatomical images of tissues with DOI, the spatial resolution cannot compete with CT or MRI. DOI and NIRS are thus functional modalities, offering similar but not identical information as fMRI, PET and SPECT. The latter methods cannot be used for continuous bedside monitoring of patients. Furthermore, MR imaging requires placing the subject in a high magnetic field, whereas in PET and SPECT the subject is exposed to irradiation from the radioactive iso-

topes injected into the bloodstream. Optical methods are well suited to bedside monitoring, completely non-invasive, and do not expose the subject to ionizing radiation. Moreover, the instrumentation can be made relatively portable or at least transportable, and can in principle be made relatively inexpensive. Optical methods are also well suited to multimodal imaging in combination with EEG or MEG measurements.

2.2 Diffuse optical imaging

Near-infrared (NIR) and visible red light in the wavelength range 650 nm to 900 nm can be used to obtain physiological information about tissue by measuring optical signal, that has travelled through the tissue between a light source (source optode) and a detector (detector optode). Most of the relevant physiological information is contained in the wavelength-dependent absorption coefficient $\mu_{\mathrm{a}}(\lambda)$ of tissue. The absorption spectra of such physiologically interesting molecules as oxygenated (HbO_2) and deoxygenated (HbR) hemoglobin vary strongly with the wavelength of the light, which makes measuring parameters such as blood content and oxygenation of tissue possible. However, the scattering of light dominates absorption in most tissues, which complicates the task of retrieving the absorption parameter from measurements. The diffuse propagation of light also limits the sensitivity in deeper structures, especially when the adult brain is studied. The physics of diffuse optical imaging is discussed in more detail in Section 3.

NIR light can be used for monitoring physiological events using single channel measurements. In brain activation imaging, the technique is called near-infrared spectroscopy (NIRS). Pulse oximetry, which is routinely used in clinical medicine, is also based on NIR light. In diffuse optical imaging (DOI), the information is processed further, in order to obtain spatially resolved images of the physiological or optical parameters. DOI requires multiple source and detector optodes.

DOI can be divided into topography and tomography. While the terminology has become somewhat blurred, the distinction between the two is generally considered to be the dimensionality: the methods, which produce two-dimensional (2D) images parallel to the plane of source and detector optodes, and with limited depth resolution, are called topography, whereas methods which reconstruct the three-dimensional (3D) spatial distribution of optical or physiological parameters, are called tomography.

2.2.1 Experimental techniques

The instrumentation needed for DOI comprises sources of NIR light, which is injected to the tissue via the source optodes, photodetectors, which receive the light from the detector optodes, and convert the intensity into an electrical signal, and amplifier, filter and analog-to-digital converter units which receive the signal from the photodetectors, and electronics for signal processing.

The types of instrumentation fall into three categories. 1. Continuous wave (CW) instrumentation requires NIR light sources which emit a signal that has either constant intensity or is modulated at a low frequency (few kHz) [5]. The measured quantity is the intensity of the signal that has passed through tissue. 2. Time domain (TD) instruments use sources which emit NIR light in short pulses (duration few ps), allowing measurement of the full time-of-flight distribution of the detected photons (temporal point spread function, TPSF) [6, 7]. 3. Frequency domain (FD) instrumentation uses high frequency modulated light sources (order of 100 MHz), and the measurables are the amplitude and phase shift in the detected signal [8, 9].

In Publications IV and V, the effect of having time-resolved information from either FD or TD instrumentation on reconstructing brain activations was studied. The results suggest that time-resolved information can help making the reconstructions

more spatially accurate and robust than if only intensity measurements from CW instrumentation are available.

2.2.2 Near-infrared spectroscopy and optical topography

The simplest method to study brain function using NIR light is NIRS, which can be performed using only a single source and a single detector. In this case, no image is formed, nor is an image reconstruction performed. In optical topography, multiple measurements are used to produce a 2D map of the physiological changes.

In NIRS and in optical topography, changes in concentrations of relevant absorbers (often HbO_2 and HbR) are assessed using the modified Beer–Lambert law, which gives the ratio of the signal intensity $A(\lambda)$ after a physiological change to original signal intensity $A_0(\lambda)$ for a wavelength λ as

$$\log\left(\frac{A(\lambda)}{A_0(\lambda)}\right) = -d \cdot DPF \cdot \sum_i \Delta C_i \alpha_i(\lambda). \tag{2.1}$$

Here d is the distance between the source and detector optodes, and DPF is the experimental *differential pathlength factor*, which accounts for the fact that due to the diffusive propagation, the average path travelled by the photons is much greater than the geometric distance. The quantities ΔC_i and $\alpha_i(\lambda)$ are the concentration change and the specific extinction coefficient of an absorber i, and the sum goes over all relevant absorbers i.

The tissue is assumed to be optically homogeneous. No spatial information is obtained in NIRS, whereas in optical topography, the change in μ_a or the concentrations of relevant absorbers as recorded by an individual measurement, is considered to be located at the midpoint between the source and detector optodes, and a 2D map is obtained by interpolating between these midpoints. Only the closest detector to each light source is considered. The resolution can never be higher than

the optode density, and very often it is poorer. Using only one measurement to assess changes in the concentrations of the absorbers at each point used for the interpolation is a likely source of inaccuracy.

2.2.3 Optical tomography

In optical tomography, the goal is to reconstruct the 3D distribution of optical properties, or changes in these properties, within tissue. Distribution of healthy and diseased tissues, or changes in physiological parameters, can then be calculated.

Propagation of NIR light in most biological tissues is highly diffusive due to high scattering of NIR light. This is illustrated in Figure 2.1. The diffusive light propagation makes reconstructing the 3D distribution of optical parameters a complicated task. To solve this *inverse problem*, one must be able to solve the *forward problem*, which is to predict propagation of NIR light in heterogeneous tissue. Solutions of the forward problem are discussed in Section 3. The aim can be either to reconstruct the absolute optical parameters, or to reconstruct the change in optical parameters (typically μ_{a}) due to, for example, a brain activation. These two approaches are called *absolute imaging* and *difference imaging*, respectively.

Absolute imaging requires multiple measurements, preferably including measurements in a diffuse transmission geometry (see Figure 2.2 a). Difference imaging can be performed using measurements of backscattered photons (diffuse reflection geometry, see Figure 2.2 b). Measurements relying on diffuse reflection are made possible by the diffusiveness of light propagation. When the optodes are placed on a relatively flat surface, the 3D space sampled by the measurement has a banana-like shape. This is illustrated in Figure 2.3.

For difference imaging, which is most often used for studying physiological changes

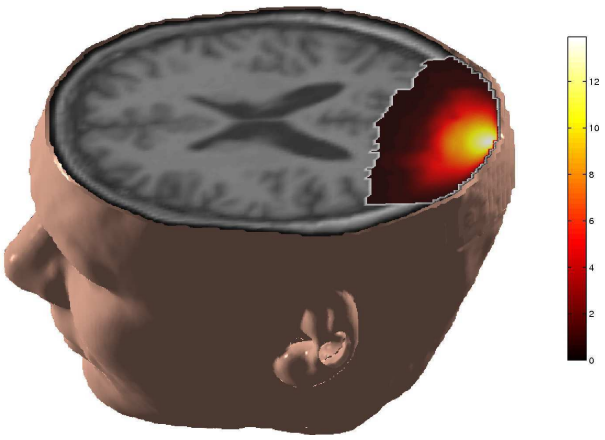

Figure 2.1: Illustration of diffuse light propagation in the human head. The image shows typical fluence of light from one light source on the back of the head. The data were calculated using Monte Carlo simulation, and are presented superimposed on the brain anatomy using arbitrary logarithmic scale (see Section 3.3.2).

due to brain activations, the modelling of the optical background is very important for accurate and reliable results. Methods for modelling the photon propagation are presented in Section 3. Optical tissue models are discussed in Section 4.

2.2.3.1 Image reconstruction

The forward problem consists in calculating simulated data y, when the positions of the source optodes q and internal optical properties x of tissue (these may include absorption and scattering coefficients, the anisotropy factor g and refractive index n, see Section 3) are known. The data y may be CW, TD or FD. The problem may be expressed as [10]

$$y = F(x; q), \tag{2.2}$$

where the operator F incorporates knowledge of the positions of the source optodes q and the NIR signal injected by them into the tissue. The inverse problem consists in finding a distribution of optical properties x which minimizes the difference between

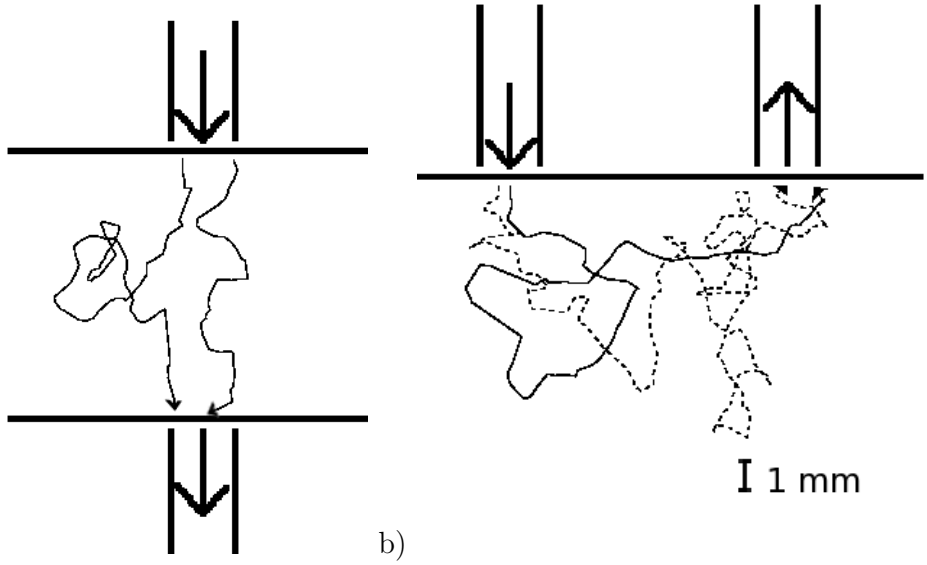

Figure 2.2: Example of optode arrangement in a) a diffuse transmission geometry measurement and b) a diffuse reflection geometry measurement. Source optode is indicated by a large arrow pointing into tissue, detector optode is indicated by a large arrow pointing outwards. In each case, routes of two photons from a 2D Monte Carlo simulation between the source and the detector are shown. The scattering parameter used in the simulation was $\mu_s = 5.0$ mm^{-1}, with anisotropy factor $g = 0.8$. This results in reduced scattering coefficient $\mu_s' = 1.0$ mm^{-1} (see Section 3.2.1). Length of 1 mm is indicated by a vertical bar.

measurements y and the solution $F(x; q)$ of the forward problem in terms of some fidelity criteria, and possibly subject to additional constraints.

The inverse problem of optical imaging is non-linear and highly *ill-posed*. Therefore in order to reconstruct the optical parameters, optimization of an objective function with respect to the parameters of a model of light propagation is required.

Linear reconstruction The function $F(x; q)$ describing the relation between the optical properties and propagation of light is non-linear, but if the optical properties x are close to an initial estimate x_0, a linearisation around x_0 may adequately ap-

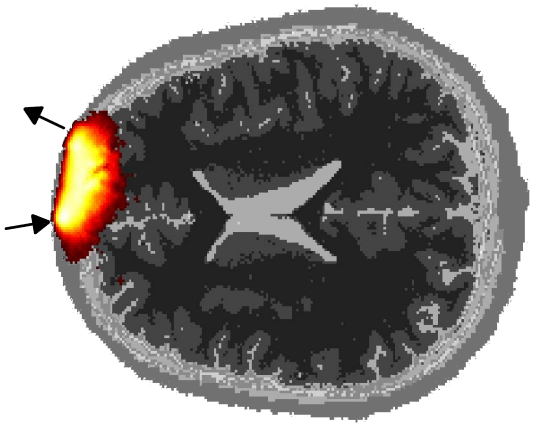

Figure 2.3: Illustration of the banana-shaped volume sampled by a measurement using one source (indicated by an arrow point into the head) and one detector optode (arrow pointing outwards) on the forehead. Shown is logarithm of photon density for photons that have travelled between the source and the detector, obtained from MC simulation (see Section 3.3.2).

proximate the situation. This approximation is typically made in difference imaging. Then Equation 2.2 can be expanded into a Taylor series around the initial estimate x_0 to obtain

$$y = F(x_0) + F'(x_0)(x - x_0) + \frac{1}{2}F''(x_0)(x - x_0)^2 ... \tag{2.3}$$

where F' and F'' are the first- and second-order Fréchet derivatives of F [11]. Equation 2.3 can be linearized by neglecting higher order terms and considering the changes in the optical properties and the data to be $\Delta x = x - x_0$ and $\Delta y = y - y_0$, respectively. Representing the Fréchet derivative F' by the Jacobian matrix $\mathbf{J}$, the linearization can be written in a matrix form as

$$\Delta y = \mathbf{J}\Delta x. \tag{2.4}$$

The inverse problem now becomes the problem of inverting $\mathbf{J}$, which may be a large, underdetermined and ill-posed problem. The matrix $\mathbf{J}$ is generally not square, and matrix pseudoinverse can be used to solve for Δx. The most commonly encountered pseudoinverse is the Moore–Penrose generalized matrix inverse [12]. Its form

depends on whether the system is overdetermined (more data elements Δy than unknown parameters Δx) or underdetermined (fewer data elements than unknown parameters). In the work presented in this thesis, high resolution reconstructions were performed, which means the problems were underdetermined. For the underdetermined case, the Moore–Penrose inverse $\mathbf{J}^\dagger$ can be written as $\mathbf{J^T}(\mathbf{JJ^T})^{-1}$ [12]. Often a regularization term is needed to make the problem stable. Further, in order to account for the varying noise levels between measurements, weighting based on the covariance of the noise can be applied. Applying the covariance based weighting and regularizing the norm of the solution Δx (Tikhonov regularization) one arrives (in the underdetermined case) at [13]

$$\Delta x = \mathbf{J^T}(\mathbf{JJ^T} + \alpha\mathbf{\Gamma})^{-1}\Delta y. \tag{2.5}$$

where α is a regularization parameter, and $\mathbf{\Gamma}$ is the covariance matrix of the measurement noise.

It is also possible to use iterative methods (based, for example on gradient descent or the Gauss–Newton algorithm) to minimize the difference between the measured Δy and Δy predicted by the linearization [14, 15]. Particularly when the number of elements in Δx (and therefore also the Jacobian $\mathbf{J}$) is very large, this may be convenient. This approach was selected in Publications IV through VI of this thesis.

Non-linear reconstruction In absolute imaging, the inverse problem is to reconstruct the absolute optical parameters, rather than merely the difference between two states. In this case, choosing a linearization point is not appropriate, and the full non-linear inverse problem has to be solved.

Non-linear image reconstruction is obtained by defining an objective function $\Phi(x)$ which represents the difference between the measured data y and the simulated data $F(x)$ obtained by solving the forward model. The set $\hat{x}$ of parameter values which

minimizes the difference is the solution to the inverse problem. Because the problem is ill-posed, a regularization term is needed.

The problem then becomes that of minimizing the function [11]

$$\Phi(x) = ||\mathbf{L}(y - F(x))||^2 + \alpha\Psi(x), \tag{2.6}$$

where $||\cdot||^2$ represents the L2-norm, and $\mathbf{L}$ is a weighting matrix. Often a diagonal matrix with the elements $L(i,i) = 1/\sigma_i$ given by the reciprocal of the standard deviation of the measurement data is chosen. The regularization term consists of a function which depends on the solution x, multiplied by regularization parameter α. The function may be as simple as $\Psi(x) = ||x||^2$, or L2-norm of x, but may also contain *a priori* information (see Section 4) to help with the reconstruction [11].

The minimization can be performed using, for example, Newton–Raphson or Levenberg–Marquart iteration. In the iteration, the forward problem is solved repeatedly.

In difference imaging using linear reconstruction, only the *difference* in the measured signal between two states is important. For reconstructing the absolute optical properties, however, the *absolute* signal must be considered. In this case, the unknown amplitude losses and phase delays (in FD) or delays in photon flight times (TD) can cause serious artefacts in the reconstructions. Calibration methods that can be included in the reconstruction have been proposed to overcome this problem [16, 17, 18].

2.2.4 Optode arrangement

In optical topography and tomography of the brain, multiple measurements are needed in order to obtain spatially resolved information. In topographic measurements, the optode grid is often designed to cover maximum area of the brain cortex

using as few source optodes as possible, for increased speed of imaging. For tomographic image reconstruction however, overlapping measurements with several source-detector distances are necessary.

In Publication V, several factors that affect image reconstruction in DOI of neonates were studied. The factor which was found to have the greatest effect on the quality of reconstructions was the density and arrangement of the optode grid. This implies that the optode grid should be carefully designed for each measurement setup for optimal results.

2.2.5 Applications in imaging brain function

First measurements of cerebral oxygenation using NIR light were reported already in 1977 [19]. Single channel NIRS has been used for measuring hemodynamic responses to brain activity in both adults and infants for over two decades, and localization of these brain responses using optical topography was first demonstrated over a decade ago [20, 11]. Functional optical imaging of both the adult and infant brain using the tomographic approach has been demonstrated within the last decade [21].

DOI has found successful applications in a wide range of functional studies of the adult brain, ranging from imaging simple visual or auditory evoked responses to studying effects that post-traumatic stress disorder has on brain responses when traumatic images are viewed [22, 23]. Additionally, the methodology is especially well-suited to imaging infants. The small size of the head makes imaging deeper structures than the superficial cortex possible. As compared to fMRI, the possibility to conduct measurements at the bed-side, using noiseless and relatively light instrumentation, and lesser sensitivity to motion artefacts are clear benefits [11]. In Figure 2.4 an optical measurement of a neonate with instrumentation developed at the Helsinki University of Technology is shown [9].

Figure 2.4: DOI of a neonate.

Applications in studies of infants include studying spontaneous brain activity [24], visual evoked activations [25], auditory evoked responses [Publication IV], passive motor activity induced responses [26], and higher brain functions, such as working memory [27]. Outside brain activation imaging, optical methods can be applied to diagnosing perinatal hypoxic-ischaemic injury, and to monitoring the efficacy of its treatment [28, 11].

3 Physics and modelling of DOI

3.1 General

NIR light interacts with biological tissues predominantly by elastic scattering and absorption. The scattering coefficient μ_s describes the average number of scattering events per unit length of distance travelled by a photon in the tissue, and the absorption coefficient μ_a represents the average number of absorption events. While obtaining physiological information is mostly based on measuring the absorption coefficient μ_a, the scattering coefficient μ_s is generally much higher, making light propagation highly diffusive. Other important optical properties are the scattering phase function $\Theta(\widehat{\mathbf{s}}, \widehat{\mathbf{s}}')$, which describes the change in direction $\widehat{\mathbf{s}}$ of photon propagation at each scattering event, and the refractive index n, which governs the speed of light in tissue.

In the wavelength range (650 to 900 nm) used by DOI, absorption of light within tissue is much lower than at either shorter or longer wavelengths. Important absorbers of NIR light in tissue are water, lipids, melanin of the skin, and hemoglobin. Absorption by water is relatively low in the wavelength range 200 to 900 nm, and rises dramatically beyond 900 nm. Absorption by lipids behaves similarly. Absorption by hemoglobin is very high below 650 nm, setting the lower limit for the DOI wavelength range. Absorption spectra of water, lipids and hemoglobin for their typical concentrations in biological tissue are shown in Figure 3.1. Optical parameters of some biological tissues are shown in Table 3.1.

Several physiologically interesting molecules have characteristic absorption spectra in the NIR wavelength range. These include oxyhemoglobin (HbO_2), deoxyhemoglobin (HbR) and cytochrome oxidase. The different spectra of HbO_2 and HbR allow determining concentrations of the oxygenated and deoxygenated forms sep-

Table 1. Optical properties of some biological tissues. Some values in the table have been calculated from the available data ($^+$), whereas other values have been approximated from graphs (*). Table is adapted from [29]. The original data are from [30, 31, 32, 33, 34, 35, 36, 37].

Tissue	μ_a (mm^{-1})	μ_s' (mm^{-1})	g	λ (nm)
Muscle (abdominal)$^+$	0.0052−0.017	0.64−0.95	-	674-956
Muscle (abdominal)$^+$	0.025−0.17	0.58−0.94	-	618-950
Muscle (back)$^+$	0.0082−0.017	0.55−1.2	-	674-956
Brain (grey matter)$^+$	0.0090−0.026	0.42−1.2	-	674-956
Brain (white matter)$^+$	0.013−0.097	0.68−1.5	-	674-956
Brain (grey matter)*	0.02−0.07	1.8−3.0	0.95-0.97	650-950
Brain (white matter)*	0.005−0.04	7−10	0.78-0.86	650-950
Brain (neonatal, grey mat)*	0.02−0.05	0.4−0.7	0.98−0.99	650-900
Brain (neonatal, white mat)*	0.03−0.05	0.7−1.3	0.97−0.98	650-900
Brain (CSF, approx. by pure water)$^+$	0.0013−0.029	~ 0	-	650-900
Blood*	0.13-0.49	2.5−4.0	0.99−0.995	665-960
Bone (pig skull)$^+$	0.022−0.052	1.2−2.8	0.91−0.96	650-950
Bone (human skull)$^+$	0.02−0.07	0.75−1.2	-	674-956
Skin (dermis, Caucasian)$^+$	0.0053−0.049	1.3−3.4	-	618-950
Skin (dermis, black)$^+$	0.025−0.46	1.1−5.5	-	617-949
Subdermal fat$^+$	0.0040−0.024	0.8−1.7	-	617-949

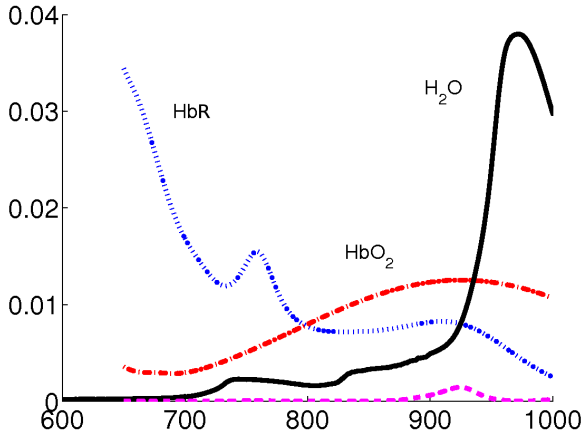

Figure 3.1: Scaled absorption coefficients of water (solid), HbR (dotted), HbO_2 (dashdot), and lipids (dashed) in the NIR region, reproduced from [29]. Data are from [33, 38, 39]. The spectra are calculated by assuming typical tissue concentrations for the absorbers (75% water content, 15% lipid content, 40 micromolar concentrations for HbR and HbO_2). On the x-axis, wavelength in nm. On the y-axis, absorption in mm^{-1}.

arately, and thus makes it possible to separately determine the total hemoglobin

concentration and the oxygenation level. The oxygenation-dependent spectra of cytochrome enzymes can be used in a similar manner. From hemoglobin concentrations, information about blood volume and oxygenation in tissue can be deduced, whereas cytochrome enzymes can be used as indicators of oxygenation of tissue [11].

The dimensions of the objects that are studied are typically much greater than the wavelength of radiation used, and they contain irregular microstructures, which cause cancellation of wave effects. Light can thus be regarded as photons, and wave effects as described by Maxwell's equations can be ignored. The diffusive nature of light propagation makes the situation fundamentally different from that applicable for methods such as computed tomography, in which the photons are usually assumed to travel in straight lines. Photons that travel through the tissue go through several scattering events, making the use of the Radon transform for image reconstruction generally infeasible. On the other hand, the fact that light propagation in most tissues is diffusive, can be exploited in modelling by approximating the radiation to be diffusive and isotropic. This approximation is not, however, valid near light sources, tissue surface, and in tissues, which exhibit anisotropy or a high ratio of absorption to scattering.

3.2 Radiative transfer equation

The radiative transfer equation (RTE) [40] is a general model of light propagation. It is a conservation equation, which states that the time derivative of the radiance (energy flow per unit volume per unit solid angle per unit time) of photons $\frac{\partial}{\partial t}\phi(\mathbf{r}, \widehat{\mathbf{s}}, t)$ in a direction $\widehat{\mathbf{s}}$ at a position $\mathbf{r}$ and time t is obtained as the sum of the term $q(\mathbf{r})$ which describes the light sources in the media and scattering of photons towards direction $\widehat{\mathbf{s}}$ minus terms describing the absorption and scattering of photons away

from direction $\widehat{\mathbf{s}}$. It can be written as [10]

$$\left(\frac{1}{c}\frac{\partial}{\partial t} + \widehat{\mathbf{s}}\cdot\nabla + \mu_{\mathrm{a}}(\mathbf{r}) + \mu_{\mathrm{s}}(\mathbf{r})\right)\phi(\mathbf{r},\widehat{\mathbf{s}},t) = \mu_{\mathrm{s}}(\mathbf{r})\int_{\mathbb{S}^2}\Theta(\widehat{\mathbf{s}},\widehat{\mathbf{s}}')\phi(\mathbf{r},\widehat{\mathbf{s}}',t)d\widehat{\mathbf{s}}' + q(\mathbf{r},\widehat{\mathbf{s}},t). \tag{3.1}$$

where $\mu_{\mathrm{a}}(\mathbf{r})$ and $\mu_{\mathrm{s}}(\mathbf{r})$ are the absorption and scattering coefficients, and $c = c_0/n$ is the speed of light in the medium (c_0 is the speed of light in a vacuum).

The scattering phase function $\Theta(\widehat{\mathbf{s}},\widehat{\mathbf{s}}')$ describes the probability density of a photon scattering from the direction $\widehat{\mathbf{s}}$ into the direction $\widehat{\mathbf{s}}'$. A commonly used phase function is the Henyey-Greenstein function [41]

$$\Theta_{HG}(\widehat{\mathbf{s}},\widehat{\mathbf{s}}') = \frac{1}{4\pi}\frac{1-g^2}{(1+g^2-2g(\widehat{\mathbf{s}}\cdot\widehat{\mathbf{s}}'))^{(3/2)}}, \tag{3.2}$$

where the *anisotropy factor* g is the mean of cosine of the scattering angle

$$g = \int_{\mathbb{S}^2}\Theta(\widehat{\mathbf{s}},\widehat{\mathbf{s}}')\times(\widehat{\mathbf{s}}\cdot\widehat{\mathbf{s}}')d\widehat{\mathbf{s}}'. \tag{3.3}$$

The Henyey-Greenstein function is a heuristic model which has been used to model scattering of photons from objects as diverse as clouds and blood cells. As it only depends on the cosine of the scattering angle, the absolute direction of photon propagation is assumed not to affect the scattering. Hence the Henyey-Greenstein function describes scattering in an *isotropic* medium. In the standard RTE, also the optical absorption and scattering parameters μ_{a} and μ_{s} are assumed to be isotropic. The assumption that light propagation in biological tissues is isotropic is reasonable in most cases. However, there are some tissues, such as axon bundles of white brain matter, which exhibit *anisotropic* structure at cellular level, and this anisotropy can be expected to affect light propagation. Modelling anisotropic light propagation is discussed in Sections 3.2.2 and 4.3 and in Publications I and II of this thesis.

The RTE treats light as photons, disregarding any wave effects. As noted above, this approximation can be made when light propagation is modelled in context of diffuse optical imaging. Above, the RTE is written assuming that the refractive index be constant. However, extensions of the RTE for spatially varying refractive index have also been presented [42, 43, 44, 45].

3.2.1 Diffusion approximation

The RTE models light propagation accurately for turbid objects of dimensions that are encountered in diffuse optical imaging. Unfortunately solving for the light field at all points of a large 3D imaging medium is computationally very expensive, and thus simpler models often need to be used. The P_N approximations to the RTE can be obtained by expanding the direction-dependent terms $\phi(r, \widehat{\mathbf{s}}, t)$, $q(\mathbf{r})$ and $\Theta(\widehat{\mathbf{s}}, \widehat{\mathbf{s}}')$ into series using spherical harmonics and keeping the N first harmonic orders. After some lengthy calculations, this yields (N+1)^2 coupled partial differential equations. Considering larger N gives progressively more accurate approximations P_N to the RTE, but with increasing computational expense [46].

The diffusion equation (DE) can be derived by starting with the P_1 approximation and making the following further approximations. First, isotropic scattering, i.e., $\Theta(\widehat{\mathbf{s}}, \widehat{\mathbf{s}}') = \Theta(\widehat{\mathbf{s}} \cdot \widehat{\mathbf{s}}')$ is assumed. Further, the light sources are assumed isotropic, and the time derivative of the photon current $\frac{\partial}{\partial t} \int \widehat{\mathbf{s}} \phi(\mathbf{r}, \widehat{\mathbf{s}}, t) d\widehat{\mathbf{s}}$ is approximated to zero. This approximation is clearly erroneous in the time-dependent case, but is usually justified by specifying the condition $\mu_\mathrm{a} \ll \mu_\mathrm{s}'$ (see below for μ_s') [10]. With these approximations, the group of four partial differential equations from the P_1 approximation can be reduced to the diffusion equation (DE)

$$\frac{1}{c}\frac{\partial}{\partial t}\Phi(\mathbf{r}, t) - \nabla \cdot \kappa_0(\mathbf{r})\nabla(\mathbf{r}, t) + \mu_\mathrm{a}(\mathbf{r})\Phi(\mathbf{r}, t) = q_0(\mathbf{r}, t), \mathbf{r} \in \Omega \tag{3.4}$$

Here $\Phi(\mathbf{r}, t)$ is the photon density (fluence) in the domain Ω, and $\kappa_0 = (1/3)/(\mu_\mathrm{a}+\mu_\mathrm{s}')$ is the diffusion coefficient. The reduced scattering coefficient is defined as $\mu_\mathrm{s}' = (1 - g)\mu_\mathrm{s}$.

The solution of Equation 3.4 requires that appropriate boundary conditions be specified. In the simplest case, the fluence at the boundary may be set to zero. This is an example of the Dirichlet boundary condition, and is physically equivalent to having a perfectly absorbing medium surrounding the domain. An alternative is to specify

that the total inward directed current is zero, corresponding to a non-scattering medium surrounding the domain, with no diffuse surface reflection. This results in the Robin boundary condition. The Robin condition can also be modified to include diffuse reflections at the boundary. A diffuse light source can be represented naturally as diffuse inward directed current at a segment of the boundary, whereas collimated light sources cannot directly be described in DE. Instead, a collimated source incident at a point on the boundary of the medium is commonly represented by a diffuse point source at depth of one scattering length ($l_s = 1/\mu_s{}'$) below the surface. This arises as the mean survival depth of an exponentially decaying line source. [10, 47]

In deriving the DE, it is assumed that $\mu_a \ll \mu_s{}'$ and that light propagation is only weakly anisotropic. While the former assumption is valid in most biological tissues, the latter is violated near sources and boundaries. However, the DE can be implemented in a computationally efficient way, and is generally considered to be an adequate approximation in many cases. It has been widely and successfully applied to modelling of diffuse optical tomography [11].

Due to approximations made in deriving the DE, it may be inaccurate when used for predicting light propagation in tissues with low $\mu_s{}'$ or high μ_a, tissues which exhibit optical anisotropy, and near light sources. In most of the applications of DOI which have been reported, the distance between the source and the detector optodes has been sufficiently large to mitigate the latter problem. However, when very dense optode grids are used, the short distance from the light source may become an issue, as is suggested by results presented in Publication V of this thesis. The problem of anisotropic tissues is discussed in Sections 3.2.2 and 4.3, and that of low-scattering tissues in Section 4.2.

3.2.2 Anisotropic RTE and DE

In the isotropic RTE, the phase function $\Theta_{iso}(\widehat{\mathbf{s}}\cdot\widehat{\mathbf{s}}', \mathbf{r})$ and scattering coefficient $\mu_{\mathrm{s}}(\mathbf{r})$ are independent of the absolute direction $\widehat{\mathbf{s}}$ of photon propagation. Anisotropy can be included in the RTE by changing the phase function into an anisotropic function $\Theta_{aniso}(\widehat{\mathbf{s}}, \widehat{\mathbf{s}}', \mathbf{r})$ [48], or by including directional dependence in the scattering coefficient $\mu_{\mathrm{s}aniso}(\mathbf{r}, \widehat{\mathbf{s}})$. The latter solution is chosen in Publications I and II of this thesis.

In deriving the DE, the propagation of light is assumed diffusive and isotropic. It is, however, possible to construct an anisotropic diffusion equation which agrees reasonably well with the corresponding anisotropic RTE [49, Publication I].

When anisotropy is modelled by making the phase function dependent on the absolute direction of photon propagation, an important question is, how to construct the anisotropic phase function. Different solutions have been proposed, which in many cases have restrictions, such as the requirement to select a main direction of anisotropy [48].

In Publication I, a RTE model (implemented with Monte Carlo) and the corresponding DE model for anisotropic light propagation are derived by assuming the scattering coefficient to be anisotropic. Physically this corresponds to the situation where the mean pathlength a photon travels, before it is scattered, depends on its direction. This solution avoids the problem of formulating an anisotropic phase function, and also has the advantage of being compatible with any value of the anisotropy factor g defined in the isotropic case.

The anisotropic RTE in Publication I is implemented by replacing the isotropic $\mu_{\mathrm{s}iso}(\mathbf{r})$ by $\mu_{\mathrm{s}aniso}(\mathbf{r}, \widehat{\mathbf{s}}) = \mu_{\mathrm{s}iso}(\mathbf{r})\widehat{\mathbf{s}}^T\mathbf{M}_{\mathbf{s}}\widehat{\mathbf{s}}$, where $\mathbf{M}_{\mathbf{s}}$ is a 3×3 tensor, which describes the direction-dependence of the scattering. An anisotropic version of the DE is then

derived using $\mu_{\mathrm{s}aniso}$ instead of $\mu_{\mathrm{s}iso}$. This results in a modification of Equation 3.4 such that the diffusion coefficient κ_0 is replaced by a *diffusion tensor* $\kappa = (1/3)[\mu_{\mathrm{a}}\mathbf{I} + (1-g)\mathbf{T}_{\mu_{\mathrm{s}}}]^{-1}$. In a special coordinate system in which the coordinate axii coincide with the eigenvectors of the matrix $\mathbf{M_s}$, the tensor $\mathbf{T}_{\mu_{\mathrm{s}}}{}'$ is given by

$$\mathbf{T}_{\mu_{\mathbf{s}}}{}' = \frac{\mu_{s,iso}}{5} \begin{bmatrix} 3\lambda_1 + \lambda_2 + \lambda_3 & 0 & 0 \\ 0 & 3\lambda_2 + \lambda_1 + \lambda_3 & 0 \\ 0 & 0 & 3\lambda_3 + \lambda_1 + \lambda_2 \end{bmatrix}. \tag{3.5}$$

Here the λ are the eigenvalues of $\mathbf{M_s}$. The tensor $\mathbf{T}_{\mu_{\mathrm{s}}}$ in an arbitrary coordinate system can be easily obtained using a rotation matrix $\mathbf{R}$, as $\mathbf{T}_{\mu_{\mathbf{s}}} = \mathbf{R}\mathbf{T}_{\mu_{\mathbf{s}}}{}'\mathbf{R}^{\mathrm{T}}$. As each diagonal component of $\mathbf{T}_{\mu_{\mathrm{s}}}{}'$ has a sum of all three eigenvalues, the anisotropy in the DE is smoother than in the RTE. On one hand, this leads to some difference between the results when the anisotropy is strong (see Publication I), but on the other hand it also prevents very anisotropic diffusion tensors which would be highly incompatible with the assumptions made in deriving the DE.

3.3 Computational models

3.3.1 Analytical modelling

The RTE or the DE can be solved analytically using Green's functions [11]. The Green's function is the solution where the source is a temporal and spatial δ-function, and other spatio-temporal forms of the source can be obtained using convolution. Unfortunately, solutions are only available for a limited range of geometries, such as simple homogeneous objects [50], homogeneous objects with a single spherical perturbation, and layered media [51, 52]. Approximate solutions have also been derived for layered media [53].

Techniques based on Green's function are commonly used for solving the forward

problem for image reconstruction, when a fast solution is desired, and the geometry can be approximated as a slab or an infinite half-space. Examples of applications include optical topography [54] and optical mammography [55].

Due to limitations in the geometries and the distribution of optical properties that can be modelled using Green's function techniques, numerical methods are needed in many cases. These can be divided into statistical (stochastic) and deterministic numerical methods, each of which have their strengths and weaknesses.

3.3.2 Monte Carlo modelling

The Monte Carlo (MC) method is the most commonly used statistical modelling method, and has become the golden standard, to which other methods are compared. The MC method implements the RTE, and naturally includes the Poisson error statistics in the solution. The MC methods have the advantage that anatomical models with arbitrary geometries can be easily implemented as can any distribution of optical properties. The main disadvantage is that computational times can be very long, especially if low statistical noise is desired.

The forward solution in MC is obtained by tracing paths of individual photons or photon packets as they are scattered and absorbed within the tissue. The rules of photon propagation in MC have been described in the literature in great detail [56, 41]. Here, a short description will be given.

Photons are launched into the tissue model at the positions of the source fibers. The model must define the value of the optical parameters at each point within the tissue. The relevant optical parameters are the scattering coefficient (μ_{s}), the absorption coefficient (μ_{a}), the refractive index (n) and the anisotropy factor (g) which appears in the scattering phase function governing the direction of photon

scattering (see Section 3.2). Arbitrary shape and arbitrary direction distribution of photons can be used for the source. In order to make the computation more efficient, many implementations of the MC method use photon packets instead of individual photons. The weight of the photon packet can be initialized to any value, but usually $w = 1$ is used.

The pathlength L of the photon until the first scattering event, is drawn from the exponential probability density $\mu_\mathrm{s} \exp(-\mu_s L)$. The absorption is handled by reducing the weight of the voxel packet by multiplying with $\exp(-\mu_a L)$ at each scattering event. The new direction of the photon after a scattering event is calculated using a phase function, discussed in Section 3.2.

The propagation of the photon is continued as described above until the photon either escapes the tissue, or the weight w of the photon falls under a predefined threshold. In the latter case a technique called "roulette" is applied [56]. In this technique, the photon is given one chance in m to continue propagation with weight mw, otherwise the photon is extinguished.

Another option for calculating the pathlength of the photon packet between scattering events, and handling the absorption, is to draw the pathlength from the probability density $\mu_\mathrm{t} \exp(-\mu_\mathrm{t} L)$, where $\mu_\mathrm{t} = \mu_\mathrm{s} + \mu_\mathrm{a}$. The absorption is then handled by multiplying the weight of the photon by $\mu_\mathrm{a}/\mu_\mathrm{t}$ at each scattering event. The difference between these two approaches is insignificant after the photon packet has travelled a few average scattering lengths (typically 1 mm), and thus for optical tomography of the brain, either one can be employed. At very short distances the results may differ, and in this case the first of the approaches described above can be expected to more closely implement the RTE, due to its continuous handling of the absorption.

In case of non-homogeneous tissue models, care must be taken to scale the path-

length between scattering events and weight reduction and to handle the possible internal reflections and refraction when the photon packet crosses a boundary between tissues with different optical properties. Implementation of the scaling and internal reflection is discussed in Publication I of this thesis.

The tissue model used in MC can be based on geometrical forms, infinite half-spaces or layers of different tissues. However, using accurate anatomical models is also possible. An elegant and simple implementation is to divide the anatomical model into rectangular voxels [57]. The voxels belonging to the anatomical model are then assigned into tissue types for which optical parameters are defined. The voxels can be arbitrarily small, so as to make the model as precise as needed.

In MC, reflection and refraction at the boundaries between tissues of different refractive index n and between tissue and air can be handled using Fresnel's formulae. When a voxel model is considered, the normal vectors of the boundaries are always parallel to one of the main coordinate axes. To obtain more realistic surface with a continuous distribution of the direction of the normal vector, a surface mesh of the boundary between tissue and air can be created. While meshing the boundaries between different tissues is also possible in principle, this may be difficult in case of complex tissue models. Using the voxel boundaries may also yield reasonable results, since the light propagation is, with some exceptions (close to sources, for example) diffusive and isotropic. It is also possible to ignore the reflections at the tissue surface. In this case, every photon that reaches the surface will escape the tissue.

3.3.2.1 Perturbation Monte Carlo

Monte Carlo based methods are generally used for solving the forward problem. They can also be used for calculating the Jacobian (or sensitivity map) for linear

image reconstruction. The perturbation Monte Carlo (pMC) [14, 58] is used in Publications III through VI. In pMC, the paths of the photon packets are used to obtain three-dimensional sensitivity maps which provide a linear estimate of the change in the optical signal in response to a change in the optical parameters at a specific location. The sensitivity maps, or Jacobian matrices in the formalism of Section 2.2.3.1, can be calculated from analytical expressions given below and data from MC simulations.

The sensitivity to changes in optical absorption can be derived from the expressions for signal intensity W, photon mean flight time $\langle t \rangle$ and phase shift φ as obtained from MC simulation. These are given by [59, Publications IV and V]

$$W = \sum_p w_p = \sum_p \exp\Big(- \sum_r \mu_\mathrm{a}(r) l_{r,p} \Big) \tag{3.6}$$

$$\langle t \rangle = \frac{\sum_p t_p w_p}{\sum_p w_p} = \frac{\sum_p t_p \exp(-\sum_r \mu_\mathrm{a}(r) l_{r,p})}{\sum_p \exp(-\sum_r \mu_\mathrm{a}(r) l_{r,p})} \tag{3.7}$$

and

$$\varphi = \mathrm{atan}(\frac{I_{Im}}{I_{Re}}) \tag{3.8}$$

$$I_{Re} = \sum_p w_p \cos(2\pi f t_p) \tag{3.9}$$

$$I_{Im} = \sum_p w_p \sin(2\pi f t_p) \tag{3.10}$$

where w_p and t_p are the intensity contribution and flight time of the photon packet p, and $\mu_\mathrm{a}(r)$ and $l_{r,p}$ are the absorption coefficient and the path length of the photon packet p in the region r of the tissue, respectively. The variables I_{Re} and I_{Im} are the real and imaginary parts of the complex amplitude, and f is the frequency of amplitude modulation in the FD data. The sum in the exponential function goes over all regions r of the tissue model.

The sensitivity of the signal to a change in μ_a in a region ρ is obtained by differentiation as [59, 60, Publications IV and V]

$$\frac{\partial W}{\partial \mu_\mathrm{a}(\rho)} = \sum_p -l_{\rho,p} \exp(-\sum_r \mu_\mathrm{a}(r) l_{r,p}) = \langle l_\rho \rangle W \tag{3.11}$$

$$\frac{\partial\langle t\rangle}{\partial\mu_{\mathrm{a}}(\rho)} = -\langle l_\rho t\rangle + \langle l_\rho\rangle\langle t\rangle, \tag{3.12}$$

and

$$\frac{\partial\varphi}{\partial\mu_a(\rho)} = \frac{1}{1+(\frac{I_{Im}}{I_{Re}})^2}(\frac{1}{I_{Re}}\frac{\partial I_{Im}}{\partial\mu_a(\rho)} - \frac{I_{Im}}{I_{Re}^2}\frac{\partial I_{Re}}{\partial\mu_a(\rho)}) \tag{3.13}$$

$$\frac{\partial I_{Re}}{\partial\mu_{\mathrm{a}}(\rho)} = \sum_p -l_{\rho,p}w_p\cos(2\pi f T_p) \tag{3.14}$$

$$\frac{\partial I_{Im}}{\partial\mu_{\mathrm{a}}(\rho)} = \sum_p -l_{\rho,p}w_p\sin(2\pi f T_p) \tag{3.15}$$

Here $\langle l_\rho\rangle$ is the average weighted photon pathlength in the region ρ and $\langle l_\rho t\rangle$ is the average pathlength of the photon packets in the region ρ, weighted with the total flight time and the final weight of the photon packets at the detector.

All quantities in Equations 3.11 through 3.15, needed to calculate the derivatives and obtain the pMC sensitivity maps, can be accumulated by MC simulation. These maps can be used for linear image reconstruction without the need to repeatedly run the computationally costly MC simulation.

3.3.3 Finite element method

Of the deterministic numerical methods for solving the forward problem, the use of finite element method (FEM, introduced into optical imaging in [61]) to solve the DE is the most widely used [11]. Other applicable methods include the finite difference method [54], the finite volume method (FVM) [62] and the boundary element method (BEM) [62, 49].

Computation using FEM/DE solutions is efficient, making non-linear image reconstruction (which requires repetitive solutions of the forward problem) feasible. FEM/DE can also be used for linear reconstruction. The drawbacks of this methodology include inability to correctly model light propagation in low-scattering tissues,

and inaccuracy near the sources. In addition, creating the finite element (FE) meshes required by the method can be difficult, as discussed in Section 3.4.

3.4 Anatomical models

Calculating the forward problem always requires an assumption of the underlying medium, or the anatomical model. Tissue models used in modelling photon propagation range from a homogeneous infinite half-space or slab to homogeneous models with realistic surface shape, and to heterogeneous anatomical models that describe both the external shape and the internal structures of the head in a realistic manner. Development of tissue models for DOI is discussed in more detail in Section 4.

In addition to defining the geometric structure and optical properties of the anatomical model, the computational method to be used must be considered. For example, methods such as FEM/DE cannot model light propagation in low-scattering tissues.

In the work presented in this thesis, the FEM/DE and MC methods were used for calculating the forward problem. They present different requirements to the anatomical model. In the case of FEM, a FE mesh is required. Creating a mesh of the complicated internal structures of the head can be difficult to implement. One solution is to use regular elements such as voxels [63], and sample the MRI data to assign tissue class labels. The resolution of such grid is limited by memory and other computational constraints. In MC, using the resolution of the original MR image is easy to implement, and the accuracy and resolution of the anatomical model are then only limited by the accuracy and resolution of the MRI data available.

An ideal computational model of the optical background should take into account all factors that significantly affect light propagation and allow sufficiently fast computation. In practice, compromises always need to be made.

4 Development of realistic optical modelling of the human head

4.1 Rationale and background

Image reconstruction from optical measurements is sensitive to the modelling of light transport in tissue. The modelling problem includes both the mathematical model of light propagation, discussed in Section 3, and the anatomical model.

The low-scattering cerebrospinal fluid (CSF) surrounding the brain and the anisotropic scattering of light in the white matter of the brain are two central issues specific to modelling photon propagation in the head. These problems place requirements on both the computational method and the anatomical model. The effects of the scattering properties of the CSF are discussed in Section 4.2, and those of anisotropic scattering in the white matter in Section 4.3.

The first topographic measurements of brain function were performed without image reconstruction by interpolating between multiple NIRS measurements [20], implicitly assuming a homogeneous semi-infinite half-space geometry. With this technique, the spatial resolution cannot be better than the optode spacing. Moreover, the NIRS technique is intended for estimating global physiological changes, and the results are often analyzed using methodology such as the modified Beer–Lambert law, which is appropriate when assessing global changes. Therefore, when changes in the brain are focal, partial volume effect can cause significant underestimation of the changes. Also, due to differential wavelength sensitivity, the relative recovered concentration changes in different chromophores can be overly sensitive to optode positions [64]. By performing image reconstruction using the DE with a homogeneous semi-infinite half-space model, both the spatial and quantitative accuracy can be improved [64].

By replacing the semi-infinite half space by a layered slab, or by a layered half-space model, the differences in optical properties between the brain and the superficial tissues (the scalp and the skull) can be accounted for [5]. When imaging specific regions of the adult brain, the optodes may be located on the scalp in such a way that a slab or a half-space may be a reasonable approximation of the underlying geometry. In infants, measurements are possible over distances that are larger relative to the size of the head, and the curvature of the head cannot be ignored. The shape of the infant head can be approximated by a sphere, the radius of which can be optimized to match the 3D locations of the optodes, if these are known [65]. However, superior reconstruction results are obtained when a realistically shaped model, which allows taking into account the exact relative positions of optodes in three dimensions, is used [66, 65, 67].

The use of slab geometry in functional imaging of adults is common [5]. In recent studies on infants, realistically shaped homogeneous models have been used [68]. However, it has been shown, that using *a priori* anatomical information, which can be derived from MR imaging, can considerably enhance the image reconstruction by making solutions of the forward problem more accurate [69, 63]. Estimates for the optical parameters of the tissues can be obtained from literature, but these are derived from various sources such as *in vitro* measurements of tissue samples or animal studies, and may not be accurate. Possible strategies for obtaining better estimates include using calibrated measured data to non-linearly reconstruct the parameters for the relevant tissue classes, starting from literature parameters and assuming piece-wise constant parameter values. The results presented in publications IV, V and VI of this thesis suggest, that using accurate anatomical knowledge for calculating the forward problem can improve reconstructions from optical measurements of infants.

In addition to making the solution of the forward problem more accurate, *a priori* anatomical information can also be incorporated into the inverse problem. This

can be done by either restricting the reconstruction to a region of interest, defined by the prior information (such as the cortex of the brain) [70, 71], or by using regularization which biases the solution towards the region of interest. A cortical constraint in reconstructing brain activations is addressed in publication IV of this thesis. However, uncertainty of the prior anatomical information and, in the case of constraining the solution to the cortex in brain activation imaging, physiological noise coming from superficial tissues, can degrade the image quality. Evaluation and minimization of this degradation remains an unsolved problem [69, 72].

4.2 Cerebrospinal fluid

The cerebrospinal fluid (CSF), which surrounds the brain and fills the ventricular system in the brain, is a clear liquid. In the region surrounding the brain, the CSF shares its space with blood vessels and the delicate network of thin fibers of the arachnoid mater, which cause some scattering. However, it is reasonable to assume that the scattering coefficient in the CSF space is low, making the space non-diffusive. The effect of the CSF layer on modelling photon propagation and reconstructing images from DOI data is a subject of active research.

To account for the effect of the CSF, both an adequate computational method and an anatomical model are needed. Implementations of the DE, which adequately describe photon propagation in most biological tissues, are widely used in DOI. However, the assumption of diffusive photon propagation made in deriving the DE does not hold in the case of the CSF. Various methods for modelling light propagation in the CSF have been proposed. The MC method can model tissues with arbitrary optical properties, but it is computationally prohibitively expensive for use in non-linear image reconstruction, at least with current desktop personal computers. The same applies to using deterministic methods to solve the RTE [62]. Other methods, which have been developed for modelling the CSF, include the hy-

brid radiosity-diffusion FEM model, which assumes the CSF to be non-scattering [73, 74, 75, 76, 77], and the hybrid RTE-DE method [78]. In the case of the relatively thin CSF layer, which surrounds the brain, it has been suggested that the use of a μ_s' value, which is low but still in the diffusive domain, is adequate for reconstructing local activations on the cortex [79].

Rather than being a simple tissue layer, the CSF space has an irregular structure formed by the sulci and gyri of the brain. In certain areas of the CSF layer surrounding the brain, the layer may be very thin, whereas in regions such as the Sylvian fissure, it may extend several centimeters into the brain. The shape of the CSF space in a neonatal head is illustrated in Figure 4.1.

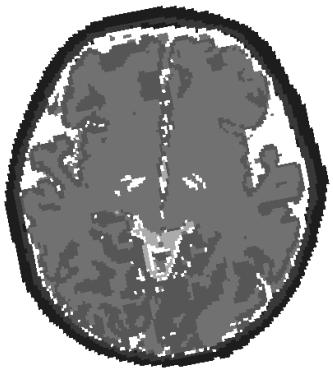

Figure 4.1: Illustration of the shape of the CSF space (shown in white) in a segmented MR image of the head of a full term neonate.

Results from simulations in Publication II indicate, that the effect of the CSF space on the absolute signal is both significant, and sensitive to the exact optode locations. In Publication V, correct modelling of the CSF was found to be important for reconstructing difference images, when the change in the absorption occurred close to a large CSF-filled sulcus.

4.3 Tissue anisotropy

Many human tissues have properties that depend on direction as well as location. Tissues such as muscle, skin and nervous tissue have anisotropic structure at the cellular level. The anisotropy of tissue has been shown by measurements to affect light-propagation in chicken breast tissue [80], human skin [81] and dentin [82]. In the brain, the axon bundles of white matter give rise to directionally dependent diffusion properties for water molecules, which can be measured by diffusion tensor (DT) MRI [83]. This has lead some researchers to believe that the propagation of NIR light may also be affected by the anisotropy, which naturally leads to the question of whether or not this effect is significant in diffuse optical imaging of the brain.

In publications I and II, the effect of tissue anisotropy on light propagation in realistic models of the adult and infant heads was studied. The anatomical models were derived from MR imaging. Information of the anisotropy was obtained from DT-MRI data, which depends on the diffusion of water. The anisotropy of photon propagation and anisotropic diffusion of water were assumed to depend on the same structures, and hence be qualitatively similar.

In the case of the adult head, the effect of tissue anisotropy on the simulated signal was found to be very small, suggesting that anisotropy can be ignored when adult subjects are imaged. In the case of an infant subject, the effect on anisotropy on the signal was significant in some simulated measurements. However, the 3D patterns of sensitivity of the optical measurements, studied in Publication II, were found to be little affected by anisotropy. This suggests that in difference imaging (such as imaging of brain function), anisotropy may not need to be considered. The effect of anisotropy on both the simulated signal and the sensitivity pattern was found to be much smaller than the effect of the non-scattering CSF layer.

The simulations presented in Publications I and II are based on the assumed similarity between the anisotropies of light propagation and water diffusion. While no confirming measurements of the assumed relation exist, it is plausible since measurements in chicken breast tissue show a preferential propagation of photons in the direction of the muscle fibers, which is also the preferential direction of the diffusion of water molecules [80]. Moreover, since DT-MRI data describes the structural anisotropy of the white matter, considered to be the basis of the anisotropy of photon migration, and fully anisotropic light propagation, with the form of the anisotropy obtained from DT-MRI, was assumed, the results of Publications I and II can be expected to give an estimate for the upper limit of the effect of anisotropy on optical measurements. The limited spatial resolution of DT-MRI, however, leads to averaging of anisotropic microstructures. Hence a more accurate result might be obtained using more precise knowledge of the anisotropic microstructure of the white matter.

4.4 Generic anatomical model

Individual MRI data of the subject provides the most accurate anatomical information that can be used for image reconstruction in DOI. The positions of the optodes should be carefully localized in the MR image. In situations, where MRI and DOI can be performed simultaneously, using MRI sensitive markers on the optodes the problem of co-registration is simplified. A simultaneous fMRI measurement provides further prior information for localizing the physiological change seen by DOI. However, simultaneous MR imaging is not always feasible, nor is individual MRI data always available. An *atlas* model which provides generic anatomical information is expected to be a valuable aid in analyzing data from optical measurements in these cases.

Use of *a priori* information derived from MR images of a single individual other than

the subject to aid image reconstruction in DOI has been studied in Publication IV in the infant case, and in Reference [84] in the case of the adult. In both cases the *a priori* anatomical model was deformed to correspond to the surface shape of the subject. However, due to variability between subjects, the use of the anatomy of one individual to model light propagation in another may cause significant errors. This suggests that a *probabilistic* atlas, based on a library of MR images, and assigning a probability for tissue classes at each point inside the head, could be more useful.

The advantages of accurate anatomical *a priori* information in optical the imaging of brain activations is explored in publication V. The construction of a probabilistic atlas of the infant head is presented in publication VI of this thesis.

Figure 4.2 illustrates how using generic anatomical *a priori* information derived from a single individual other than the subject may cause error in the reconstruction. Reconstructing activations in the auditory cortex of a neonate was studied using MC simulation as explained in Publication VI. A focal brain activation was simulated by introducing a localized absorptive perturbation into the brain. The perturbation was reconstructed from simulated difference data using the pMC method with three different background models. These were the reference model, in which the difference data were generated (the simulated subject), the probabilistic atlas, and an anatomically realistic model derived from MR imaging of a single individual other than the simulated subject. The latter model is called here the 'wrong' reference model. Both the atlas and the 'wrong' reference model were deformed to correspond exactly to the surface shape of the subject (the reference model). Accurate knowledge of the optical parameters of the tissue classes was assumed. From Figure 4.2 it can be seen that while all models are able to correctly localize the brain activation, in the reconstruction obtained using the 'wrong' reference model, a strong absorption change appears to the right of the perturbation. This artefact, which is caused by noise in the simulated data, is present also in the other two perturbations, but as a much weaker change. The result shows that use of inaccurate prior information can,

in some cases, cause significant artefacts in the reconstruction. The use of realistic anatomical *a priori* information is explained in more detail in Publications III-V, and the use of the probabilistic atlas is explained in Publication VI.

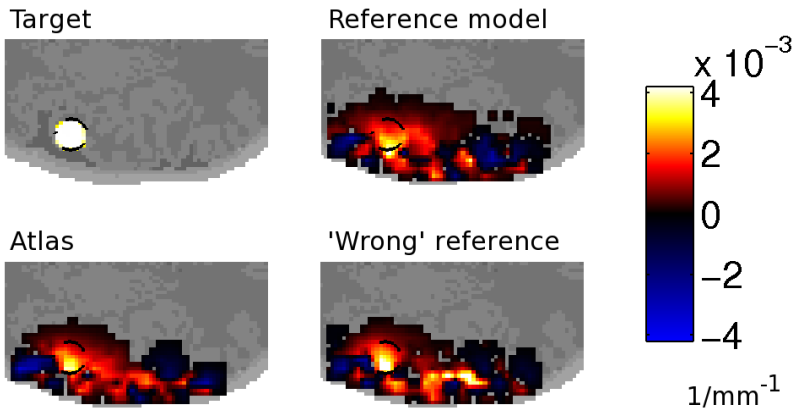

Figure 4.2: Reconstruction of an absorption change. Axial slices through the center of the simulated absorptive perturbation are shown. The simulated perturbation ('Target') had contrast 5.5 mm^{-1} from the background. The reconstructions obtained using anatomical information from the reference model, the atlas, and the "wrong" reference model are shown (explained in the text).

4.4.1 Creating a probabilistic atlas

The requirements for creating a probabilistic atlas of the human head are

1. A library of accurate anatomical information from individuals belonging to the targeted subject population

2. The segmentation of the individual anatomical images

3. The co-registration of the individual anatomical images to a common geometry, using only the surface shape of the head and anatomical landmarks

4.4.1.1 Obtaining anatomical data

MR imaging can be used to obtain accurate anatomical information. In Publication VI, the construction of a probabilistic atlas for use with full term neonates is presented. In this group, the gestational ages of the subjects from which the library information is derived should be closely (to within few weeks) the same as that as the subjects whose data will be analyzed using the atlas. Care should be taken if an atlas constructed from images of full term neonates is used in optical imaging of preterm infants. Preferably an atlas constructed from MR images of preterm infants with similar gestational ages should be used. In general, the data used for creating the atlas should be representative of the anatomical variation of the subject population the atlas is intended to be used with.

The effect of the CSF (discussed in Section 4.2) on image reconstruction is greatly influenced by the thickness of the CSF layer. As the CSF functions as a cushion between the skull and the brain cortex, its local thickness and distribution depends on the position of the head. Therefore for optimal results, the subjects used in the library of anatomical information should be imaged in the same position as the subjects whose data will be analyzed using the atlas.

Another consideration in obtaining the MR images is the selection of optimal MR imaging sequences. The sequence should be able to distinguish between gray and white brain matter and between the skull and the scalp, and to accurately separate the CSF from other tissues. The optimal sequences depend on the age group of the subjects. In case of infants, the sequence should be fast and resistant to artefacts induced by movements, often present in MRI data of young children. Suitable approaches for obtaining library data of infants are the FLASH [85] and FISP [86] sequences [87]. In the adult case, quality of MR images is generally good, and choosing optimal imaging sequences is less critical. However, having both T1 and T2 weighted data will aid in segmenting the images.

4.4.1.2 Segmentation of MR images

Many automatic or semi-automatic segmentation tools exist for segmenting the adult human brain [88, 89]. However, these tools generally do not segment the superficial structures, which are important when the MRI data is used to solve the forward problem of DOI. Furthermore, as these methods have been designed for the adult brain, they generally perform poorly with MR images of the infant head.

For this reason, the MR images of infants used in Publications II and IV through VI were segmented manually, using interactive software developed by the co-authors. To ensure good quality, also the final steps in segmenting the adult MR images, used in Publications I and III, were done manually, using commercial software [90].

Obviously, if a large number of MR images are to be segmented, automatic, or at least semi-automatic, methods are preferable. One possibility is to co-register the individual MR images to a pre-segmented image, thus automatically obtaining a segmentation for each image. A drawback of this method is that presumably some variation in the locations of small sulci would be lost, and the result might exhibit some of the individual features of the segmented base image. Most of the research on automatic co-registration of MR images concentrates on co-registering the brain.While this allows a good segmentation of the brain, the superficial tissues would need to be segmented separately if such a co-registration is used to support the segmentation of the entire head.

4.4.1.3 Co-registration of MR images

An atlas, that is used as a source of anatomical *a priori* information in DOI, should contain information about the variability of the spatial distribution of tissues inside the head. This information should include the variability present in the thickness

of the scalp, skull and the CSF layers, and the positions of major sulci and other internal structures, which may affect the propagation of light. The shape of the outer surface of all the co-registered images in the atlas should be the same, in order to achieve an unambiguous external boundary. To achieve this, the co-registration should be based on the external shape of the head, and on the positions of anatomical landmarks on the scalp. Co-registering the brain and forcing the superficial tissues to have the same thickness would result in the loss of important information about the anatomical variability. In Publication VI of this thesis, the atlas model was created by using only surface shape and anatomical landmarks on the scalp for the co-registration.

4.4.1.4 Optical parameters

The atlas only contains information about the spatial distribution of tissues in the head. For modelling light propagation, optical parameters have to be assigned to the tissues. Values obtained from the literature may be used as a starting point. However, these may be inaccurate. In Publications V and VI the effect of moderate inaccuracy of the optical parameters was studied in the case of perfect anatomical knowledge, and in the case where the atlas was used. Results from linear reconstruction of difference images remained good with moderately inaccurate optical parameters for the tissue types, but the quality of the reconstructions is expected to be compromised, if larger errors are present.

Methods for reconstructing the accurate optical parameters of different tissues from optical measurements should be studied to address this problem. While the problem of deriving the absolute optical parameters from measurement data is severely ill-posed, limiting the dimension of the problem to finding parameters for a limited number of tissue classes instead of performing unconstrained reconstruction of the spatial distribution, could make the problem more tractable.

5 Discussion

In this thesis, the modelling of NIR light propagation in the human head was studied. The aim of the research was to evaluate the significance of various aspects of the modelling in reconstructing functional images from DOI data and to create modelling methods to improve such reconstructions. In addition, the significance of the experimental setup was considered.

Two problems specific to the problem of DOI studies of the brain are the presence of low-scattering CSF and the anisotropic structures formed by the axon bundles in the white matter of the brain.

In Publications I and II, the significance of the possible anisotropic scattering of light the white brain matter was studied in case of the adult and infant heads, respectively. In the infant case, the assumed effect of optical anisotropy on the NIR signal was compared to that of the CSF. The results suggest that the effect of anisotropy in imaging of adults is small. It was found that in infants the anisotropy can have a significant effect on the measured optical signal, but the results suggest that the significance in image reconstruction from difference imaging data is small, and can probably be ignored. Moreover, the effect of the CSF was found to be much greater than that of the anisotropy. The effect of the CSF for the reconstruction of difference images was explored in Publication V, with the result that while large pools of CSF such as in the larger sulci of the brain can have significant effect on reconstructions, thinner layers of CSF have less effect, and can be approximated by relatively low-scattering but still diffusive optical parameters, that can be modelled with DE.

In Publications III through VI, linear reconstruction using the pMC method, and the significance of accurate knowledge of the optical background were studied in the

context of difference imaging. The results suggest that inaccuracy in the modelling of the optical background, be it in the anatomical model or approximations in the computational model, can lead to poor accuracy or even failure of the reconstructions in cases where more accurate modelling can produce good results. Anatomical *a priori* knowledge was found to significantly improve the accuracy and robustness of image reconstruction. This result holds even when the prior knowledge of the optical parameters of various tissue classes is moderately inaccurate, but obviously use of very inaccurate optical parameters changes the situation. Anatomical knowledge derived from a single individual, deformed to correspond to the head shape of the subject, was found to improve image reconstruction in some cases. However, the variation in brain anatomy between normal subjects suggests that superior results can obtained with a probabilistic atlas model based on multiple MR images. The construction of such a model is presented in Publication VI.

In Publications IV and V, the significance of time-resolved data-types from FD or TD instrumentation was studied. In Publication V the effect of the optode arrangement on brain activation imaging was explored by comparing three optode grids that were similar to arrangements proposed in literature. The density of the optode grid was found to be decisive in reconstructing focal activations in the cortex of a neonate, while the availability of time-resolved data was found to significantly improve the spatial accuracy and robustness of image reconstruction. The results suggest that for imaging brain activations in neonates, the optode grid should have a spatial sensitivity pattern which is as uniform as possible and there should be multiple overlapping measurements covering the region of interest. If measuring TD or FD data with a dense multi-distance optode grid, good signal-to-noise ratio and a sufficiently short imaging time is possible, this will lead to best reconstruction results. If compromises need to be made, the results of Publication V suggest that for accurate and reliable reconstruction of focal brain activations, a sufficiently dense optode grid is the most important factor. Theoretically, optimal density of the optode grid is such that further increasing the density of optodes does not increase

information content from what can be achieved by simply interpolating between measurements. In Publication V it was found that if imaging time is not considered, an optode grid with inter-optode distance less than one centimeter allows best image quality of reconstructions.

The imaging of the infant brain is an attractive application of DOI. While in the adult, the limited sensitivity to deeper tissues restricts the method to imaging the superficial cortex, the smaller size of the infant head makes imaging deeper structures possible. The results presented in this thesis indicate that accurate modelling of the optical properties of the head can significantly improve the reconstructed images, and can in some cases be crucial for obtaining a successful reconstruction. When accurate anatomical information such as MR image of the subject is available, this should be used to aid the reconstruction. For cases where such information is not available, age-group specific atlas models should be developed.

Optical parameters used with the anatomical models should be carefully selected. As a starting point, parameter values derived from literature can be used, however, these may be inaccurate. Ideally, the piecewise continuous optical parameters of the tissue classes should be reconstructed from measurement data. The difficult task of reconstructing absolute optical parameters will hopefully be alleviated to some degree by only reconstructing parameters of relatively few tissue classes rather than trying to solve the full spatial distribution of tissue parameters from measurement data alone. Physiological changes can then be reconstructed with high spatial resolution using sensitivity maps obtained with the recovered optical parameters of the tissue classes, and linear reconstruction. In using an accurate anatomical model, correctly co-registering the positions of the optodes with the model is an important consideration. The effect of inaccurate co-registration was, however, not studied in this thesis.

In this thesis, accurate modelling of NIR light propagation was studied, and an atlas

model for DOI in infants was developed. The results of Publication VI constitute a proof of concept for the atlas model. Future work should include constructing age- and subject-group specific atlases using a sufficient number of constituent MR images, and developing methods for finding the surface shape of a subject and co-registering the atlas to this shape, and for reconstructing the optical parameters of the tissue classes in the atlas using measured data.

6 Summary of the publications

Publication I

In this Publication, a new method was presented for modelling light propagation in anisotropically scattering tissues in 3D, and the anisotropic RTE and the corresponding DE were presented. A Monte Carlo model capable of describing photon migration in arbitrary geometry with spatially varying optical properties and tissue anisotropy was implemented. Relation between anisotropic diffusion of water as recorded by DT-MRI and anisotropic light propagation was proposed, and anisotropic light propagation was studied in a realistic MRI based model of the adult human head. Results of this simulation study suggested that the significance of anisotopic tissues in DOI of adults be small.

Publication II

Using the methodology developed in Publication I, anisotropic light propagation in the infant head was studied. T1- and DT-MRI data was used for constructing realistic anisotropic optical models of newborn infants. The results suggest that while tissue anisotropy may have a significant effect on the absolute data recorded in diffuse transmission measurements, which are possible on small infants, the effect on difference imaging is small, and much smaller than the effect of the low-scattering space occupied by CSF.

Publication III

A high resolution pMC method for diffuse optical tomography was implemented, and the use of linear pMC reconstruction studied. DOI was used to record hemodynamic changes due to visual activations in the adult brain. Reconstruction of

the hemodynamic changes was studied using simulated and measured data, and the effect of using cortical constraint in the reconstruction was explored. The results show that in the case of adult subjects, even a strong hemodynamic change may be difficult to localize accurately without constraining the solution.

The main reasons for the difficulty of reconstructing brain activations in the adult case are that the sensitivity of measurements is limited to the very superficial cortical areas, and the poor contrast-to-noise (CNR) ratio of measurements. CNR is defined here as the ratio of the contrast in the difference data caused by brain activation to the noise in the measurement. The noise level in the simulations presented in the publication was similar to the noise level in real measurements. In the simulations, the noise in the signal intensity was approximately 0.2% at 10 mm and 1 % at 30 mm source-detector-separation.

Publication IV

In this Publication, the implementation of the pMC methodology introduced in Publication III was expanded to use FD data. Auditory activations of the infant brain were studied using DOI. The significance for the reconstruction of accurate *a priori* information of the optical background and of having both phase and amplitude data types from FD measurements instead of intensity data from CW measurements alone were studied using simulated data. The pMC method and a FEM/DE based method were used for reconstructing the 3D distribution of changes in HbO_2 from measured data, and the results were compared. Temporal data provided by FD measurements and *a priori* knowledge of the optical background were found to improve reconstructions significantly.

An optode arrangement consisting of a single source and multiple detectors was used in this study. The simple grid is not well-suited for tomographical imaging, which limits the generalizability of the results. The results show, however, that

anatomically realistic *a priori* information can be beneficial when only few optodes are used.

Publication V

The Publications treats the issues of the significance of accurate knowledge of the optical background properties and the use of time-resolved information in reconstructing images of hemodynamic changes in the neonatal brain from DOI data. The effect of the optode layout was also investigated. The results suggest that the design and especially the density of the optode grid is decisive for obtaining good reconstructions. The use of time-resolved information significantly improved the spatial accuracy. Adequate knowledge and modelling of the optical background was found to be very important for both the spatial accuracy and robustness of the reconstruction.

Publication VI

This Publication presents a deformable probabilistic atlas of the neonatal head that can be used for image reconstruction in DOI. The requirements for a useful atlas and methodology of creating such an atlas are discussed. Simulations are used to explore the utility of atlas information in reconstructing localized brain activations, and results are compared to those obtained using simpler models. Results suggest that the use of accurate anatomical a priori information can significantly enhance reconstruction results. The use of exact anatomical information specific to the subject is preferable, but when this is not available, an atlas or a layered model derived from an atlas can be used.

References

[1] S. Webb (editor), The Physics of Medical Imaging. Institute of Physics. (1992)

[2] B. R. Rosen, H. J. Aronen, K. K. Kwong, J. W. Belliveau, L. M. Hamberg, and J. A. Fordham, "Advances in clinical neuroimaging - functional MR-imaging techniques", Radiographics **13**, 889–896. (1993)

[3] D. Cohen, "Magnetoencephalography: Evidence of magnetic fields produced by alpha-rhytm currents", Science **161**, 784–786. (1968)

[4] M. Hämäläinen, R. Hari, R. J. Ilmoniemi, J. Knuutila, and O. V. Lounasmaa, "Magnetoencephalography - theory, instrumentation and applications to non-invasive studies of the working human brain", Reviews of Modern Physics **65**, no. 2, 413–497. (1993)

[5] B. W. Zeff, B. R. White, H. Dehghani, B. L. Schlaggar, and J. P. Culver, "Retinotopic mapping of adult human visual cortex with high-density diffuse optical tomography", Proc. Nat. Acad. Sci **104**, 12169–12174. (2007)

[6] F. E. W. Schmidt, M. E. Fry, E. M. Hillman, J. C. Hebden, and D. T. Delpy, "A 32-channel time-resolved instrument for medical optical tomography", Rev. Sci. Instrum. **71**, 256–265. (2000)

[7] J. Selb, D. K. Joseph, and D. A. Boas, "Time-gated optical system for depth-resolved functional brain imaging", J. Biomed. Opt. **11**, page 044008. (2006)

[8] T. O. McBride, B. W. Pogue, S. Jiang, U. L. Österberg, and K. D. Paulsen, "A parallel-detection frequency-domain near-infrared tomography system for hemoglobin imaging of the breast in vivo", Rev. Sci. Instrum. **72**, 1817–1824. (2001)

[9] I. Nissilä, K. Kotilahti, K. Fallström, and T. Katila, "Instrumentation for the accurate measurement of phase and amplitude in optical tomography", Rev. Sci. Instrum. **73**, 3306–3312. (2002)

[10] S. R. Arridge, "Optical tomography in medical imaging", Inverse Problems **15**, R41–R93. (1999)

[11] A. Gibson, J. C. Hebden, and S. R. Arridge, "Recent advances in diffuse optical imaging", Phys. Med. Biol. **50**, R1–R43. (2005)

[12] H. W. Engl, M. Hanke, and A. Neubauer, Regularization of inverse problems. Kluwer Academic Publishers, Dordrecht, Netherlands. (1996)

[13] Simon R. Arridge and John C. Schotland, "Optical tomography: forward and inverse problems", Inverse Problems (accepted for publication), (2009)

[14] C. K. Hayakawa, J. Spanier, F. Bevilacqua, A. K. Dunn, J. S. You, B. J. Tromberg, and V. Venugopalan, "Perturbation Monte Carlo methods to solve inverse photon migration problems in heterogeneous tissues", Opt. Lett. **26**, 1335–1337. (2001)

[15] I. Seo, J. S. You, C. K. Hayakawa, and V. Venugopalan, "Perturbation and differential Monte Carlo methods for measurement of optical properties in a layered epithelial tissue model", J. Biomed. Opt. **12**, 014030–1–15. (2007)

[16] D. A. Boas, T. Gaudette, and S. R. Arridge, "Simultaneous imaging and optode calibration with diffuse optical tomography", Optics Express **5**, 263–270. (2001)

[17] T. Tarvainen, V. Kolehmainen, M. Vauhkonen, A. Vanne, A. P. Gibson, M. Schweiger, S. R. Arridge, and J. P. Kaipio, "Computational calibration method for optical tomography", Appl. Opt. **44**, 1879–1888. (2005)

[18] M. Schweiger, I. Nissilä, D. A. Boas, and S. R. Arridge, "Image reconstruction in optical tomography in the presence of coupling errors", Appl. Opt. 2743–2756. (2007)

[19] F. F. Jöbsis, "Noninvasive infrared monitoring of cerebral and myocardial oxygen sufficiency and circulatory parameters", Science **198**, 1264–1267. (1977)

[20] G. Gratton, P. M. Corballis, E. Cho, M. Fabiani, and D. C. Hood, "Shades of grey matter: noninvasive optical images of human brain responses during visual stimulation", Psychophysiology **50**, 561–571. (1995)

[21] D. A. Benaron, S. R. Hintz, A. Villringer, D. Boas, A. Kleinschmidt, J. Frahm, C. Hirth, H. Obrig, J. C. van Houten, E. L. Kermit, W.-F Cheong, and D. K. Stevenson, "Noninvasive Functional Imaging of Human Brain Using Light", J Cerebral Blood Flow & Metabolism **20**, 469–477. (2000)

[22] Y. Hoshi, "Functional near-infrared optical imaging: Utility and limitations in human brain mapping", Psychophysiology **40**, 511–520. (2002)

[23] K. Matsuo, T. Kato, K. Taneichi, A. Matsumoto, T. Ohtani, T. Hamamoto, H. Yamasue, Y. Sakano, T. Sasaki, M. Sadamatsu, A. Iwanami, N. Asukai, and N. Kato, "Activation of the prefrontal cortex to trauma-related stimuli measured by near-infrared spectroscopy in posttraumatic stress disorder due to terrorism", Psychophysiology **40**, 492–500. (2003)

[24] G. Taga, Y. Konishi, A. Maki, T. Tachibana, M. Fujiwara, and H. Koizumi, "Spontaneous oscillation of oxy- and deoxy-hemoglobin changes with a phase difference throughout the occipital cortex of newborn infants observed using non-invasive optical topography", Neurosci. Lett. **282**, 101–104. (2000)

[25] G. Taga, K. Asakawa, A. Maki, Y. Konishi, and H. Koizumi, "Brain imaging in awake infants by near-infrared optical topography", Proc. Natl Acad. Sci. **100**, 10722–10727. (2003)

[26] S. R. Hintz, D. A. Benaron, A. Zourabian, D. K. Stevenson, and D. Boas, "Bedside functional imaging of the premature infant brain during passive motor activation", J Perinat. Med. **29**, 335–343. (2001)

[27] S. Tsujimoto, T. Yamamoto, H. Kawaguchi, H. Koizumi, and T. Sawaguchi, "Prefrontal cortical activation associated with working memory in adults and preschool children: an event-related optical topography study", Cererb. Cortex **14**, 703–712. (2004)

[28] M. Thoresen, "Cooling the newborn after asphyxia -physiological and experimental background and its clinical use", Semin. Neonatol. **5**, 61–73. (2000)

[29] I. Nissilä, T. Noponen, J. Heino, T. Kajava, and T. Katila, "Diffuse Optical Imaging", In: J. C. Lin (editor), Advances in Electromagnetic Fields in Living Tissue, volume 4, 77–130. Springer Science. (2005)

[30] W. Cheong, S. A. Prahl, and A. J. Welch, "A review of the optical properties of biological tissues", IEEE J. Quant. Elec. **26**, 2166–2185. (1990)

[31] M. Firbank and D. T. Delpy, "A design for a stable and reproducible phantom for use in near-infrared imaging and spectroscopy", Phys. Med. Biol. **38**, 847–853. (1993)

[32] P. Van der Zee, M. Essenpreis, and D. T. Delpy, "Optical properties of brain tissue", In: Proc. SPIE, volume 1888, 454–465. (1993)

[33] S. J. Matcher, M. Cope, and D. T. Delpy, "Use of the water absorption spectrum to quantify tissue chromophore concentration changes in near infrared spectroscopy", Phys. Med. Biol. **39**, 177–196. (1994)

[34] J. B. Fishkin, O. Coquoz, E. R. Anderson, M. Brenner, and B. J. Tromber, "Frequency domain photon migration measurements of normal and malignant tissue optical properties in a human subject", Appl. Opt. **36**, 10–20. (1997)

[35] C. R. Simpson, M. Kohl, M. Essenpreis, and M. Cope, "Near Infrared optical properties of ex-vivo human skin and sub-cutaneous tissues measured using the Monte Carlo inversion technique", Phys. Med. Biol. **43**, 2465–2478. (1998)

[36] F. Bevilacqua, D. Piguet, P. Marquet, J. D. Gross, J. D. Tromberg, and C. Depeursinge, "*In vivo* local determination of tissue optical properties: applications to human brain", Appl. Opt. **38**, 4939–4950. (1999)

[37] A. T. Lovell, J. C. Hebden, J. C. Goldstone, and M. Cope, "Determination of the transport scatter coefficient of red blood cells", In: Proc. SPIE, volume 3597, 175–182. (1999)

[38] M. Cope, The Development of a Near Infrared Spectroscopy System and its Application for Non Invasive Monitoring of Cerebral Blood and Tissue Oxygenation in the Newborn Infant, Ph.D. thesis, University of London. (1991)

[39] V. Quaresima, S. J. Matcher, and M. Ferrari, "Identification and Quantification of Intrinsic Optical Contrast for Near-Infrared Mammography", Photochem. Photobiol. **67**, 4–14. (1998)

[40] S. Chandrasekhar (editor), Radiative Transfer. Dover Publications, New York, NY, USA. (1960)

[41] L. Wang, S. L. Jacques, and L. Zheng, "MCML-Monte Carlo modeling of light transport in multi-layered tissues", Computer Methods and Programs in Biomedicine **47**, 131–146. (1995)

[42] H. A. Ferwenda, "The radiative transfer equation for scattering media with a spatially varying refractive index", Journal of Optics A: Pure and Applied Optics **1**, L1–L2. (1999)

[43] L. Marti-Lopez, J. Bouza-Dominguez, J. C. Hebden, S. R. Arridge, and R. A. Martinez-Celirio, "Validity conditions for the radiative transfer equation", Journal of Optical Society of America A **20**, 2046–2056. (2003)

[44] J.-M. Tualle and E. Tinet, "Derivation of the radiative transfer equation for scattering media with a spatially varying refractive index", Optics Communications **228**, 33–38. (2003)

[45] M. Premaratne, E. Premaratne, and A. J. Lowery, "The photon transport equation for turbid biological media with spatially varying isotropic refractive index", Phys. Med. Biol. **50**, R1–R43. (2005)

[46] E. D. Aydin, C. R. E. Oliveira, and A. J. H. Goddard, "A comparison between transport and diffusion calculations using a finite element-spherical harmonics radiation transoport methos", Medical Physics **29**, 2013–2023. (2002)

[47] M. Schweiger, S. R. Arridge, M. Hiraoka, and D. T. Delpy, "The finite element method for the propagation of light in scattering media: Boundary and source conditions", Med. Phys. **22**, 1779–1792. (1995)

[48] J. Heino and E. Somersalo, "Estimation of optical absorption in anisotropic background", Inverse Problems **18**, 559–573. (2002)

[49] J. Heino, S.R. Arridge, J. Sikora, and E. Somersalo, "Anisotropic effects in highly scattering media", Physical Review E **68**, page 031908. (2003)

[50] S. R. Arridge, M. Cope, and D. T. Delpy, "The theoretical basis for the determination of optical pathlengths in tissue: temporal and frequency analysis", Phys. Med. Biol. **37**, 1531–1559. (1992)

[51] Jean-Michel Tualle, Jérôme Prat, Eric Tinet, and Sigrid Avrillier, "Real-space Green's function calculation for the solution of the diffusion equation in stratified turbid media", J. Opt. Soc. Am. A **17**, no. 11, 2046–2055. URL `http://josaa.osa.org/abstract.cfm?URI=josaa-17-11-2046`. (2000)

[52] Mini Das, Chen Xu, and Quing Zhu, "Analytical solution for light propagation in a two-layer tissue structure with a tilted interface for breast imaging", Appl. Opt. **45**, no. 20, 5027–5036. URL `http://ao.osa.org/abstract.cfm?URI=ao-45-20-5027`. (2006)

[53] F. Martelli, A. Sassaroli, Y. Yamada, and G. Zaccanti, "Analytical approximate solutions of the time-domain diffusion equation in layered slabs", J. Opt. Soc. Am. A **19**, 71–80. (2002)

[54] J. P. Culver, R. Choe, M. J. Holboke, L. Zubkov, T. Durduran, A. Slemp, V. Ntziachristos, B. Chance, and A. G. Yodh, "Three-dimensional diffuse optical tomography in the parallel plane transmission geometry: evaluation of a hybrid frequency domain/continuous wave clinical system for breast imaging", Medical Physics **30**, 235–247. (2003)

[55] A. Torricelli, L. Spinelli, A. Pifferi, P. Taroni, R. Cubeddu, and G. M. Danesini, "Use of a nonlinear perturbation approach for in vivo breast lesion characterization by multi-wavelength time-resolved optical mammography", Optics Express **11**, 853–867. (2003)

[56] S. A. Prahl, M. Keijzer, S. L. Jacques, and A. J. Welch, "A Monte Carlo model of light propagation in tissue", In: G. J. Müller and D. H. Sliney (editors), Dosimetry of Laser Radiation in Medicine and Biology, volume 5, 102–111. SPIE IS. (1989)

[57] D. A. Boas, J. P. Culver, J. J. Stott, and A. K. Dunn, "Three dimensional Monte Carlo code for photon migration through complex heterogenous media including the adult human head", Optics Express **10**, 159–170. (2002)

[58] P. Kumar and R. M. Vasu, "Reconstruction of optical properties of low-scattering tissue using derivative estimated through perturbation Monte-Carlo method", J. Biomed. Opt. **9**, 1002–1012. (2004)

[59] J. Steinbrink, H. Wabnitz, H. Obrig, A. Villringer, and H. Rinneberg, "Determining changes in NIR absorption using a layered model of the human head", Phys. Med. Biol. **46**, 879–896. (2001)

[60] S. R. Arridge, "Photon measurement density functions: I. Analytical forms", Applied Optics **34**, 7395–7409. (1995)

[61] S. R. Arridge, M. Schweiger, M. Hiraoka, and D. T. Delpy, "Finite element approach for modelling photon transport in tissue", Medical Physics **20**, 299–309. (1993)

[62] K. Ren, G. S. Abdoulaev, G. Bal, and A. H. Hielscher, "Algorithm for solving the equation of radiative transfer in the frequency domain", Opt. Lett. **29**, 578–580. (2004)

[63] M. Schweiger, A. Gibson, and S. R. Arridge, "Computational aspects of diffuse optical tomography", IEEE Computing in Science and Engineering 33–41. (2003)

[64] D. A. Boas, T. Gaudette, G. Strangman, X. Cheng, J. J. A. Marota, and J. B. Mandeville, "The accuracy of near infrared spectroscopy and imaging during focal changes in cerebral hemodynamics", NeuroImage **13**, 76–90. (2001)

[65] A. P. Gibson, R. Md. Yusof, H. Dehghani, J. Riley N. Everdell, R. Richards, J. C. Hebden, M. Schweiger, S. R. Arridge, and D. T. Delpy, "Optical tomography of a realistic neonatal head phantom", Appl. Opt. **42**, 3109–3116. (2003)

[66] A. Y. Bluestone, G. Abdouleav, C. H. Schmitz, R. L. Barbour, and A. H. Hielscher, "Three-dimensional optical tomography of hemodynamics in the human head", Opt. Express **9**, 272–286. (2001)

[67] H. Dehghani, B. W. Pogue, S. P. Poplack, and K. D. Paulsen, "Multiwavelength three-dimensional near-infrared tomography of the breast, initial simulation, phantom and clinical results", Applied Optics **42**, 135–145. (2004)

[68] A. P. Gibson, T. Austin, N. L. Everdell, M. Schweiger, S. R. Arridge, J. H. Meek, J. S. Wyatt, D. T. Delpy, and J. C. Hebden, "Three-dimensional whole-head optical tomography of passive motor evoked responses in the neonate", NeuroImage **30**, 521–528. (2006)

[69] M. Schweiger and S. R. Arridge, "Optical tomographic reconstruction in a complex head model using *a priori* region boundary information", Phys. Med. Biol. **44**, 2703–2721. (1999)

[70] D. A. Boas, A. M. Dale, and M. A. Franceschini, "Diffuse optical imaging of brain activation: approaches to optimizing image sensitivity, resolution and accuracy", NeuroImage **23**, 275–288. (2004)

[71] D. A. Boas and A. M. Dale, "Simulation study of magnetic resonance imaging-guided cortically constrained diffuse optical tomography of human brain function", Appl. Opt. **44**, 1957–1967. (2005)

[72] A. P. Gibson, J. Riley, J. C. Hebden, S. R. Arridge, and D. T. Delpy, "A method for generating patient-specific finite element meshes for head modeling", Phys. Med. Biol. **48**, 481–495. (2003)

[73] E. Okada, M. Firbank, M. Schweiger, S. R. Arridge, M. Cope, and D. T. Delpy, "Theoretical and experimental investigation of near-infrared light propagation in a model of the adult head", Appl. Opt. **50**, 21–31. (1997)

[74] H. Dehghani, S. R. Arridge, M. Schweiger, and D. T. Delpy, "Optical tomography in the presence of void regions", J. Opt. Soc. Am. A **17**, 1659–1670. (2000)

[75] J. Riley, H. Dehghani, M. Schweiger, S. R. Arridge, J. Ripoll, and M. Nieto-Vesperinas, "3D optical tomography in the presence of void regions", Optics Express **7**, 462–467. (2000)

[76] H. Dehghani and D. T. Delpy, "Linear single-step image reconstruction in the presence of nonscattering regions", J. Opt. Soc. Am. A **19**, 1662–1671. (2002)

[77] A. Gibson, J. C. Hebden, , J. Riley, N. Everdell, M. SChweiger, S. R. Arridge, and D. T. Delpy, "Linear and nonlinear reconstruction for optical tomography of phantoms with nonscattering regions", Appl. Opt. **55**, 3925–3936. (2005)

[78] T. Tarvainen, M. Vauhkonen, V. Kolehmainen, and J. P. Kaipio, "Hybrid radiative-transfer-diffusion model for optical tomography", Appl. Opt. **44**, 876–886. (2005)

[79] A. Custo, W. M. Wells III, A. H. Barnett, E. M. C. Hillman, and D. A. Boas, "Effective scattering coefficient of the cerebral spinal fluid in adult head models for diffuse optical imaging", Appl. Opt. **45**, 4747–4755. (2006)

[80] G. Marquez, L. H. Wang, S.-P. Lin, J. A. Schwartz, and S. L. Tahomsen, "Anisotropy in the absorption and scattering spectra of chicken breast tissue", Appl. Opt. **37**, 798–804. (1998)

[81] S. Nickell, M. Hermann, M. Essenpreis, T. J. Farrell, U. Krämer, and M. S. Patterson, "Anisotropy of light propagation in human skin", Phys. Med. Biol. **45**, 2873–2886. (2000)

[82] A. Kienle, F. K. Forster, R. Diebolder, and H. Hibst, "Light propagation in dentin: influence of microstructure on anisotropy", Phys. Med. Biol. **48**, N7–N14. (2003)

[83] P. J. Basser, J. Mattiello, and D. Le Bihan, "MR diffusion tensor spectroscopy and imaging", Biophys. J. **66**, 259–267. (1994)

[84] A. Custo, Purely Optical Tomography: Atlas-Based Reconstruction of Brain Activation, Ph.D. thesis, Massachusetts Institute of Technology. (2008)

[85] A. Haase, J. Frahm, D. Matthaei, W. Hänicke, and K. D. Merboldt, "FLASH imaging: rapid NMR imaging using low flip angle pulses", J. Magn. Res. **67**, 258–266. (1986)

[86] A. Oppelt, R. Graumann, and A. Barfuss, "FISP: a new fast MRI sequence", Electromedia (English edn) **3**, 15–18. (1986)

[87] R. Sepponen. "Oral communication". (2008)

[88] B. Fischl, D. H. Salat, E. Busa, M. Albert, M. Dieterich, C. Haselgrove, A. van der Kouwe, R. Killiany, D. Kennedy, S. Klaveness, A. Montillo, N. Makris, B. Rosen, and A. M. Dale, "Whole Brain Segmentation: Automated Labeling of Neuroanatomical Structures in the Human Brain", Neuron **33**, 341–355. (2002)

[89] B. Patenaude, S. Smith, D. Kennedy, , and M. Jenkinson, "FIRST - FMRIB's Integrated Registration and Segmentation Tool", In: Proc. Human Brain Mapping, 2007. (2007)

[90] Elekta Neuromag, Helsinki, Finland